Sources and atmospheric processing of wintertime aerosols in Seoul, Korea: Insights from real-time measurements using a high-resolution aerosol mass spectrometer

Hwajin Kim[1,2], Qi Zhang[3,4*], Gwi-Nam Bae[1,2], Jin Young Kim[1,2], Seung Bok Lee[1]

[1] Center for Environment, Health and Welfare Research, Korea Institute of Science and Technology, Seoul, Korea

[2] Department of Energy and Environmental Engineering, University of Science and Technology, Daejeon, Korea

[3] Department of Environmental Toxicology, University of California, Davis, CA 95616, USA

[4] Department of Environmental Science and Engineering, Fudan University, Shanghai, China.

*Corresponding author: Qi Zhang

Department of Environmental Toxicology, University of California 1 Shields Avenue, Davis, California 95616

Phone: (530)-752-5779

Email: dkwzhang@ucdavis.edu

Abstract

Highly time-resolved chemical characterization of non-refractory submicrometer particulate matter (NR-PM_1) was conducted in Seoul, the capital and largest metropolis of Korea, using an Aerodyne high-resolution time-of-flight aerosol mass spectrometer (HR-ToF-AMS). The measurements were performed during winter, when elevated particulate matter (PM) pollution events are often observed. This is the first time that detailed real-time aerosol measurement results are reported from Seoul, Korea, which reveal valuable insights into the sources and atmospheric processes that contribute to PM pollution in this region.

The average concentration of submicron aerosol (PM_1 = NR-PM_1 + black carbon (BC)) was 27.5 μg m^{-3}, and the total mass was dominated by organics (44%), followed by nitrate (24%) and sulfate (10%). The average atomic ratios of oxygen-to-carbon (O/C), hydrogen-to-carbon (H/C), and nitrogen-to-carbon (N/C) of organic aerosol (OA) were 0.37, 1.79, and 0.018, respectively, which gives that average organic mass-to-carbon (OM/OC) ratio of 1.67. The concentrations (2.6–90.7 μg m^{-3}) and composition of PM_1 varied dynamically during the measurement period, due to the influences of different meteorological conditions, emission sources, and air mass origins. Five distinct sources of OA were identified via positive matrix factorization (PMF) analysis of the HR-ToF-AMS data: vehicle emissions represented by a hydrocarbon like OA factor (HOA; O/C = 0.06), cooking activities represented by a cooking OA factor (COA; O/C = 0.14), wood combustion represented by a biomass burning OA factor (BBOA; O/C = 0.34), and secondary organic aerosol (SOA) represented by a semi-volatile oxygenated OA factor (SV-OOA; O/C = 0.56) and a low volatility oxygenated OA factor (LV-OOA; O/C = 0.68). On average, primary OA (POA = HOA + COA + BBOA) accounted for 59% the OA mass whereas SV-OOA and LV-OOA contributed 15% and 26%, respectively.

Our results indicate that air quality in Seoul during winter is influenced strongly by secondary aerosol formation with sulfate, nitrate, ammonium, SV-OOA, and LV-OOA together accounting for 64% of the PM_1 mass during this study. However, aerosol sources and composition were found to be significantly different between clean and polluted periods. During stagnant periods with low wind speed (WS) and high relative humidity (RH), PM concentration was generally high (average ± 1σ = 43.6 ± 12.4 μg m^{-3}) with enhanced fractions of nitrate (27%) and SV-OOA (8%), which suggested a strong influence from local production of secondary aerosol. Low PM loading periods (12.6 ± 7.1 μg m^{-3}) tended to occurred under higher WS and lower RH conditions and appeared to be more strongly influenced by regional air masses, as indicated by higher mass fractions of sulfate (12%) and LV-OOA (20%) in PM_1. Overall, our results indicate that PM pollutants in urban Korea originate from complex emission sources and atmospheric processes and that their concentrations and composition are controlled by various factors including meteorological conditions, local anthropogenic emissions, and upwind sources.

1 Introduction

Ambient aerosols can reduce visibility, damage human health, and influence climate change directly by absorbing and reflecting solar radiation, and indirectly by modifying cloud formation and properties (IPCC, 2013;Pope III and Dockery, 2006;Pöschl, 2005). Elevated particulate matter (PM) pollution in urban areas are known to arise due to anthropogenic emissions and stagnant meteorological conditions (Cao et al., 2012;Guo et al., 2014;Sun et al., 2014).

Seoul is one of the most populated and developed city in Korea and is facing a severe PM pollution problem. The annual average concentration of $PM_{2.5}$ in Seoul decreased from 28.5 μg m^{-3} in 2005 to 22.5 μg m^{-3} in 2012 since the enactment of the "Special Act on Seoul Metropolitan Air Quality Improvement" in 2005, which has led to emission reduction from diesel vehicles and fugitive dust emissions on road and open area (Kang et al., 2016;KOSAE, 2009). However, the amount of reduction was not dramatic and the annual average $PM_{2.5}$ concentration increased again in 2013 to 24.8 μg m^{-3}. These values far exceeded the $PM_{2.5}$ annual standards set by the USA (15 μg m^{-3}) and the WHO (10 μg m^{-3}). Due to growing concerns over the adverse effects of atmospheric PM, the South Korean government established $PM_{2.5}$ standards in 2015: 25 μg m^{-3} for annual average and 50 μg m^{-3} for 24-hr average (NIER, 2014).

Mitigating air pollution in Seoul remains a great challenge because it remains unclear which emission sources and atmospheric process are responsible for the problem (Harrison and Yin, 2000), despite numerous studies that have focused on these issues worldwide (e.g., Ervens et al., 2011;Gelencsér et al., 2007;Jimenez et al., 2009;Ng et al., 2010;Young et al., 2016;Zhang et al., 2007a). A main reason is the complexity of ambient aerosols, which have a range of chemical compositions and originate from a wide range of sources and atmospheric processes (Seinfeld and Pandis, 2006). Furthermore, several recent studies investigate the impacts of meteorology on air pollution as well (Ding et al., 2013;Ding et al., 2016;Petaja et al., 2016). For example, high PM concentration was found to happen more frequently during winter due to a combination of factors, including elevated emissions from primary sources for heating, lower boundary layer (BL) height, and stagnant meteorological conditions, which favor the accumulation of PM and secondary aerosol precursors (Hennigan et al., 2009). In addition, cold weather in winter promotes the gas-to-particle partitioning of semi-volatile species such as nitrate. In addition, since Seoul is located downwind from the Asian Continent, where concentrations of ambient aerosols have increased significantly in recent years (Huang et al., 2014;Liu et al., 2013;Quan et al., 2011), long-range

transport of pollutants from upwind polluted areas often influences air quality in Seoul, especially during winter (Kim et al., 2014). As a result, both local and regional sources contribute to high concentrations of PM, both separately and in combination (Heo et al., 2009), making air quality control more difficult. Therefore, understanding the sources and processes responsible for PM composition and concentration is critical for the public to recognize regional haze events and to enact effective PM reduction strategies for Korea as well as for the broader northern pan-Eurasian region (Liu et al., 2013). Also, from a global point of view, studies of atmospheric PM pollution may contribute to a better understanding of the Earth system science and enacting efficient climate policy (Kulmala et al., 2015).

Most previous aerosol studies in Korea were based on offline sampling which involves filter collection followed by laboratory analyses. However, a main drawback of this method is low time-resolution which limits our ability to perform detail investigations on the atmospheric evolution processes. Furthermore, organic aerosol (OA) analysis conducted in Korea has so far focused on molecular level, which led to the identification of a small portion of the OA mass (Choi et al., 2012;Choi et al., 2016). Aerosol mass spectrometers (AMS) have been widely used in recent years because they allow for chemical speciation, sizing and the mass detection of non-refractory submicrometer particulate matter (NR-PM_1), with a high time resolution (Canagaratna et al., 2007). Furthermore, using multivariate analysis methods (Zhang et al., 2011), the OA was decomposed into several sources such as hydrocarbon-like OA (HOA), biomass burning OA (BBOA), cooking-related OA (COA), coal combustion OA (CCOA), and oxygenated OA (OOA). In addition, the OOA factor has been further separated according to volatility, e.g., low volatility fraction (LV-OOA) and a semi-volatile fraction (SV-OOA) or oxidation, e.g., more oxidized (MO-OOA) and less oxidized (LO-OOA) (e.g., Lanz et al., 2007;Parworth et al., 2015;Setyan et al., 2012;Aiken et al., 2008;Huang et al., 2011;Mohr et al., 2012). These studies have identified the sources, constituents and the evolution process of PM which is critical for establishing efficient control strategies and model representations (Ulbrich et al., 2009;Zhang et al., 2011).

Many AMS studies have been conducted in East Asia including China, Hong Kong, and Japan, but a detailed PM characterization using AMS has not yet been reported in Seoul, Korea (Li et al., 2015 and references therein). In this study, we deployed a high-resolution time-of-flight aerosol mass spectrometer (HR-ToF-AMS), manufactured by Aerodyne Research Inc. (Billerica, MA, USA), in Seoul for 6 weeks (from December 5, 2015 to January 21, 2016) to characterize

wintertime NR-PM_1 in this urban area. We particularly focus on aerosol properties, sources, and processes in winter, when the weather was generally cold and relatively dry during the day but was humid during the night. Our goal was to use detailed information obtained from in situ measurements to facilitate a fundamental understanding of the formation processes and emission sources of atmospheric aerosols in Seoul, which may improve our understandings on what factors and how they influences urban air quality. This information will eventually allow for the design of better pollution abatement strategies and improved parameterizations in air quality models. Here, we report: (1) the mass concentrations, size distributions, chemical composition, and temporal and diurnal variations of PM_1 species; (2) the characteristics and dynamic variations of OA sources and processes using PMF; and (3) the characteristics, sources, and impact factors of the PM_1 composition and OA components on polluted and unpolluted days.

2 Experimental Methods

2.1 Sampling site description

Seoul, the capital of Korea, is located in the central-west of the Korean Peninsula surrounded by the Yellow Sea. Korea is generally under the influence of a prevailing north-westerly wind bringing air masses originating from mainland China during winter (Fig. 1). In this study, real-time measurements of particle composition and size distribution were conducted at the Korea Institute of Science and Technology (KIST) located in the northeast of Seoul (37.60N, 127.05E), 7 km from the center of Seoul. The sampling was conducted on the 5^{th} floor of one of the KIST buildings (60 m above sea level). As shown in Fig. 1d, KIST is located ~ 400 m from a busy highway and is surrounded by a residential area, forest and a commercial area, suggesting that the air quality at the site tends to be influenced by abundant anthropogenic and primary sources. There are no major industrial or wood burning sources in the vicinity of KIST. However, in the west and west south part of Seoul, ~ 35 km away from the measurement site (Fig. 1b), there are a number of industrial facilities that are significant anthropogenic sources for SO_x and the highest emission rate range was measured at 4856-17222 ton/year. There are also sporadic agricultural areas surrounding the city of Seoul (e.g., Gyeonggi Province), where open biomass burning often times occurs during winter. A wide range of meteorological and air quality data were also collected from a separate supersite located at 500 m away from the northwest of the KIST.

2.2 Measurements

The NR-PM_1 chemical components including sulfate, nitrate, ammonium, chloride, and organics as well as their size distributions were measured by an Aerodyne HR-ToF-AMS (DeCarlo et al., 2006) at a time resolution of 2.5 min. The black carbon (BC) concentration was measured with a multi angle absorption photometer (MAAP; Thermo Fisher Scientific, Waltham, MA, USA). Both instruments sampled downstream of a $PM_{2.5}$ cyclone (URG Corp.; Chapel Hill, NC, USA). The number size distributions of aerosols with mobility sizes between 20.9–947.5 nm were measured by a scanning mobility particle sizer (SMPS 3080; TSI Inc., St Paul, MN, USA). The hourly concentration of trace gas (e.g., CO, O_3, NO_2 and SO_2) measured at Gireum site (37.61N, 127.03E) were acquired from the Korea Environment Cooperation (KECO) (http://www.airkorea.or.kr). Meteorological measurement data such as ambient temperature, relative humidity (RH), wind speed and wind direction were obtained from the nearby Jungreung site (37.61N, 127.00E) maintained by the Korea meteorological administration (http://www.kma.go.kr). The data reported in this paper are in local time, which is Korea Standard Time (KST) and is 9 h earlier than the Universal Coordinated Time (UTC).

In this study, the HR-ToF-AMS was operated in the standard configuration and obtained mass spectra (MS) and efficient particle time of flight (ePToF) data. Furthermore, the HR-ToF-AMS was operated under the 'V' and 'W' modes, where high sensitivity but low mass resolution was achieved in 'V' mode, and low sensitivity, but high mass resolution was achieved in 'W' mode. Ionization efficiency (IE) and particle sizing calibrations were performed following standard protocols (Canagaratna et al., 2007) before, during, and after the measurement period.

2.3 AMS data analysis

2.3.1 Basic HR-ToF-AMS data analysis

HR-ToF-AMS data were processed and analyzed using the standard toolkit (SeQUential Igor data RetRiEval (SQUIRREL; ver. 1.57I), and PIKA (ver. 1.16I; available for download at http://cires.colorado.edu/jimenez-group/ToFAMSResources/ToFSoftware/index.html)) within Igor Pro (Wavemetrics, Lake Oswego, OR, USA). Details on the data processing procedures have been described in previous studies (Aiken et al., 2008;Aiken et al., 2009;Allan et al., 2004). Briefly, the standard fragmentation table described by Allan et al. (2004) was used, with some small modifications to process the raw MS. The modifications were based on data from four

filtered air measurements. This allowed measurements of the background from the gas-phase signal, which needed to be removed from the particle-phase measurement. Adjustments were made to the measured CO_2^+ (m/z = 44) signal to remove the contributions from gas phase CO_2 as well as the $^{16}O^+$ to $^{14}N^+$ ratio for air signals at m/z = 29 based on measurements of particle-free ambient air. Relative ionization efficiencies (RIE) of 1.1, 1.075, and 3.875 were used for nitrate, sulfate, and ammonium, respectively, based on values determined from calibrations using pure NH_4NO_3 and $(NH_4)_2SO_4$ aerosols. A composition-dependent collection efficiency (CDCE) was applied to the data based on an algorithm by Middlebrook et al. (2012). Nitrate was observed to be an important component of NR-PM_1 during this study (24%), although the campaign average (± 1σ) CE was 0.5 ± 0.02. Furthermore, the total concentrations of particle-bound polycyclic aromatic hydrocarbons (PAHs) were estimated using the method described in Dzepina et al. (2007). However, instead of apportioning the unit mass resolution (UMR) spectra, PAH-related ions were determined via fitting the high-resolution mass spectra (W-mode) (Xu et al., 2014). In addition, a RIE of 1.35 with respect to nitrate was applied to calculate mass concentrations of PAHs from AMS data (Dzepina et al., 2007).

The quantification of NR-PM_1 species was validated through comparisons between the total PM_1 mass (PM_1 = NR-PM_1 + BC) and the apparent particle volume measured by the SMPS (Fig. 2e, Fig. S1a). As shown in Fig. S1a, the SMPS-measured particle volume correlated strongly with the AMS measured total mass (R^2 = 0.9). From this strong correlation, the inter-comparison of AMS mass versus SMPS volume yielded a slope of 1.22, which was lower than the average particle density of 1.46 estimated using the measured chemical composition in this study (Zhang et al., 2005b) (Fig.3c and Fig. S1b). Note that the average organic aerosol density was estimated to be 1.12 based on elemental ratios (Kuwata et al., 2012). The evolution pattern of the AMS total mass-based size distribution also compared well with the volume-based size distribution from SMPS measurements throughout the day (Fig. S1c,d). The detection limits of the main chemical components in AMS are listed in Table 1, and are typically far lower than the observed concentrations. All the reported mass concentrations from AMS in this study are based on ambient conditions.

The elemental ratios between oxygen, carbon, hydrogen, nitrogen and sulfur as well as the organic mass to carbon ratio (OM/OC) of OA, were determined from an analysis of the W mode high resolution mass spectra (HRMS) data, following the method recently reported by Canagaratna et

al. (2015). The elemental ratios calculated using the Aiken-Ambient method (Aiken et al., 2008) are detailed in Table S1 along with the ratios calculated using the Canagaratna method for comparison. Unless otherwise indicated, the O/C, H/C, and OM/OC ratios stated in this paper from other studies have been calculated using the updated elemental analysis method (Canagaratna et al., 2015). Note that there could be biases in the S/C ratios since no correction factor is available.

2.3.2 Positive Matrix Factorization (PMF) Analysis

The HRMS of organic aerosol were analyzed using PMF. The analysis was performed using the PMF2 algorithm in robust mode (Paatero and Tapper, 1994), with the PMF Evaluation Toolkit (PET ver 2.05) (Ulbrich et al., 2009), which was downloaded from http://cires1.colorado.edu/jimenez-group/wiki/index.php/PMF-AMS_Analysis_Guide#PMF_Evaluation_Tool_Software. The data and error matrices were prepared according to the protocol described by Ulbrich et al. (2009) and outlined in Table 1 of Zhang et al. (2011). In brief, a minimum error value was applied to the error matrix and each ion was assessed and treated according to their signal-to-noise ratio (SNR). Ions with an average SNR of less than 0.2 were removed, and those with SNR between 0.2 and 2 were downweighted by increasing their errors by a factor of two. Further, ions related to *m/z* 44 (i.e., CO_2^+, CO^+, H_2O^+, HO^+, and O^+) were also downweighted to avoid overestimating the importance of CO_2^+. Isotopes were removed from the matrices because their signals were scaled to their parent ions rather than being measured directly. After these treatments, the resulting matrix consisted of 286 ions between *m/z*'s 12 and 120.

PMF was applied to the data and the number of factors (*p*) in the solution was explored from one up to nine. Although the PMF algorithm was able to provide a number of mathematically sound solutions, in order to obtain physically meaningful results, several criteria were used to evaluate and select the appropriate number of factors from the model. The recommendations outlined in Zhang et al. (2011) including an investigation of the key diagnostic plots, mass spectral signatures, diurnal profiles, and correlations with external tracers, were followed to assess the results and determine the number of factors.

The rotational ambiguity of each of the solution sets was explored by varying the fPeak parameter from -1 to 1, with an increment of 0.1. The five factor solution with fPeak = 0 ($Q/Q_{exp} = 2.56$), was selected for further analyses because it satisfied the above criteria, including a good separation of the temporal and mass spectral variations of the five factors. A summary of the key diagnostics is

presented in Fig. S2 in the Supplement. The five factor solution was found to be very stable as the mass fraction of each of the factors remained relatively constant between fPeaks -0.4 and +0.2 (Fig. S2c). Fig. S3 shows the mass spectra and the time series of the four and six factor solutions; where factor 1 and factor 2 in the four factor solution set could be identified as low volatility OA (LV-OOA) and semi-volatile OA (SV-OOA), respectively based on the O/C ratio, but were both highly oxidized, with a higher fraction of *m/z* 44 than *m/z* 43. Moreover, all factors in this solution set showed the signature of biomass burning OA (BBOA) at *m/z* 60 and *m/z* 73, indicating that more factors may be needed to resolve the mixed factors. In contrast, the temporal variations from the six factor solution were similar to those from the five factor solution set but showed indications of factor splitting. For example, two very similar BBOA-like factors (factors 3 and 4) were identified in the six factor solution, where the main difference was that factor 4 had a higher N/C ratio than factor 3. Although different types of BBOA sources are possible, we did not have external evidence to validate the separation. Furthermore, given the fact that having only one BBOA factor (i.e., the five factor solution set) did not influence the separation of the other factors, it was not necessary to go for higher number of factors. Consequently, the five factor solution, which resolved HOA, COA, BBOA and two types of OOA, was chosen as it appears to best represent OA sources and processes in Seoul during winter.

2.4 Backtrajectory and Bivariate conditional probability function analysis

In this study, 96-h back trajectories were calculated every hour using version 4.9 of the Hybrid Single-Particle Lagrangian Integrated Trajectory (HYSPLIT) model (Draxler, 2012;Draxler, 1997) for the sampling periods from December 5, 2015 to January 21, 2016. The trajectories were released at half of the mixing height at the KIST (latitude: 37.60N; longitude: 127.05E) and the average arriving height for the back trajectories for this study was approximately 191 m. To identify the pollutant characteristics in different predominant transport patterns, cluster analysis was performed on the trajectories using the software HYSPLIT4 and 4 clustered were identified according to their similarity in a spatial distribution. Individual back trajectories in each cluster are shown in Fig. S12.

In addition, conditional probability function (CPF) (Kim et al., 2003) was performed to estimate the local sources and their impacts on PM_1 composition and individual organic aerosol sources from PMF analysis, using wind directions coupled with the concentration time series of each species. The CPF plots represent the probability that a specific compound or source is located in

certain wind direction, assisting to find the local point source. The directional origin of regionally transported sources may not be consistent with the local surface wind data used for the CPF plots due to the tophography of the region (Heo et al., 2009).

3 Results and discussion

3.1 Overall characteristics

3.1.1 Temporal variations of PM_1 composition and chemical properties

The overall characteristics and temporal variations of wintertime PM_1 in Seoul, including mass and volume concentrations, and size distributions are shown in Fig. 2, along with the time series of gaseous pollutants, e.g., CO, SO_2, and O_x ($O_x = O_3 + NO_2$), and meteorological conditions (RH, temperature, wind direction, wind speed). From Dec. 6, 2015 to Jan. 21, 2016, the average concentration of PM_1 (= NR-PM_1 + BC) was 27.5 μg m^{-3}, ranging from 2.6 to 90 μg m^{-3}. Assuming that PM_1 represents approximately 80% of $PM_{2.5}$ mass (Lim et al., 2012), we found that 29% of the measurement days (i.e., 14 days) violated the National Institute of Environmental Research (NIER)'s daily $PM_{2.5}$ standards (50 μg m^{-3}) and 58% of the days (28 days) violated the WHO's daily standard (25 μg m^{-3}). Although severe haze with high PM_1 concentration close to 90 μg m^{-3} was observed several times, the averaged mass concentration of PM_1 (27.5 μg m^{-3}) was still moderate because of the frequent occurrence of clean periods in winter. The average concentration of PM_1 measured in Korea during this study was similar to or slightly lower than those measured during wintertime in several urban areas in China, including Shanghai (Huang et al., 2012), Shenzhen (He et al., 2011), Lanzhou (Xu et al., 2016), and Hong Kong (Li et al., 2015), but was much lower than in Beijing where the wintertime mass concentrations of PM_1 were found to be 7-10 times higher than in Seoul (Sun et al., 2014).

The large variations in PM_1 mass concentrations (2.6 to 90 μg m^{-3}; Fig. 2e) and other pollutants (Fig. 2c), such as CO (0.3 to 2.3 ppm), O_3 (3 to 46 ppb), and NO_2 (8 to 98 ppb), reflected that air quality in Seoul is influenced by dynamic changes in emission sources, atmospheric processes, as well as meteorological conditions. In addition, new particle events were observed during this study and they showed characteristics of a sharp increase of ultrafine particle number concentration and subsequent growth of these particles in size (Fig.2j). This finding is the first time in urban area of Korea, although frequent (~7.4 % of the measurement days) observations of new particle formation

and growth events were reported from the 3 year continuous measurements using SMPS at Gosan station (33.17N, 126.10E) which is pristine rural area but downwind site of Asian Continent facing yellow Sea (Kim et al., 2013).

Based on the variations of PM_1 concentrations and meteorological conditions (Fig. 2), we divided the whole study into two typical periods: (1) high loading period (daily $PM_1 > 30$ μg m^{-3}) and (2) low loading period (daily $PM_1 < 14$ μg m^{-3}). 30 and 14 μg m^{-3} correspond to the middle values of the PM_1 concentrations estimated based on the NIER and WHO daily and yearly $PM_{2.5}$ standards, respectively. As shown in Figs. 2 and 3, high and low loading periods usually alternated during winter in Seoul. Comparisons between the high and low loading periods can indicate how different sources and atmospheric processes influence air quality in this region. Details on the periodic variations of air quality in Seoul are discussed at section 3.4.

On average, OA was the largest component of the PM_1, accounting for 44% of the total mass, followed by nitrate (24%), sulfate (10%), ammonium (12%), BC (9%) and chloride (1%) (Fig. 3a, 4a and Table 1). POA (= HOA + COA + BBOA) and SOA (= SV-OOA + LV-OOA) accounted for 59 and 41%, respectively, of OA mass (section 3.3). Consequently, ~ 36% of PM_1 was consisted of primary materials (POA + BC), with the remainder (64%) being secondary species (NO_3^- + SO_4^{2-} + NH_4^+ + SOA), indicating that the aerosol pollution problem in Seoul during wintertime was more strongly influenced by secondary aerosol formation processes. Details on the sources and processes that led to severe air quality are discussed in section 3.4.

The molar equivalent ratios of total inorganic anions to cation for NR-PM_1 (= (SO_4^{2-}/48 + NO_3^-/62 + Cl^-/35.5) / (NH_4^+/18)) were close to 1; thus, submicron aerosols were mostly neutralized in the forms of ammonium salts, such as NH_4NO_3, $(NH_4)_2SO_4$, and NH_4Cl (Zhang et al., 2007b) (Figs. 3d and 4b). Possible sources of ammonium in Seoul include on-road vehicle emissions, neutralizer using in industry, and agricultural emissions at the outskirt of Seoul. Note that particles appeared to have "excess" NH_4^+ at high organic aerosol loadings (Fig. 4b), probably due to the presence of carboxylate ions, such as formate, acetate, and oxalate, which were not counted in the calculation of ion balance (Ge et al., 2012b). Further investigations of this issue might be necessary in the future.

3.1.2 Diurnal patterns of PM_1 composition

Diurnal patterns can provide insights into aerosol sources and formation processes. In this study, the daily variations in concentrations of aerosol species show distinctively different patterns, indicating that the sources and formation processes of PM pollutants in Seoul were diverse and complex. First, secondary inorganic species, such as sulfate, nitrate, and ammonium, all displayed different diurnal profiles. In the case of nitrate (Fig. 5c), the daily variations started to increase at ~ 07:00, peaked at midday (10:00-12:00), and then slowly decreased until 17:00. Previous studies (Brown et al., 2006;Lurmann et al., 2006;Sun et al., 2012;Young et al., 2016;Xu et al., 2014) have attributed this type of daytime peak shortly after sunrise to the mixing-down of secondary aerosols formed at night in a residual layer aloft. Later, the photochemical formation of nitrate from NO_x, emitted from rush hour traffic, contributed to an increase in nitrate concentration during daytime, a feature of regionally generated secondary inorganic species. The decreasing trend afternoon is likely due to the evaporative loss of semi-volatile species at higher air temperatures as well as the dilution effects due to the enhanced BL height in the afternoon. Significant amount of nitrate can also be formed through nighttime chemistry, as indicated by the high fractional contribution during night (Fig. 5f). Given that somewhat high concentrations of O_3 (~12.0 ppb) and NO_2 (~41.7 ppb) were observed during night time (18:00 – 6:00) (Fig. S10), nitrate formation from N_2O_5 hydrolysis possibly occurred.

Unlike nitrate, sulfate concentration was elevated during nighttime, showing a trend that started to increase from late afternoon (~16:00), peaked at around 10:00 on the following day, and then gradually decreased afterwards to reach a minimum value at 16:00 (Fig.5b, Fig.6b). The overnight increase starting in the late afternoon appeared to be associated with enhanced gas-to-particle partitioning of SO_2 and aqueous phase processing facilitated by the relatively low temperature and high RH at night (Fig. 6). Indeed, fSO_4 (= the ratio in sulfate (SO_4^{2-}) to SO_x (SO_4^{2-} + SO_2) based on sulfur contents (Kaneyasu et al., 1995)) increased during night time and showed relatively good correlation with RH (R^2 = 0.59, Fig. 6a). However, fSO_4 started to decrease at ~6:00 (Fig. 6c) but sulfate concentration continued to increase till 10:00 (Fig. 6b). This increase of sulfate concentration appeared to be due to a similar reason as that of nitrate – mixing with the higher concentration of sulfate in the upper residual layer formed at night. The residual layer was also enriched of SO_2 (Fig. 6b), for which nighttime transport of air mass from industrial facilities located on the west (Fig. S11) and southwest outskirts of Seoul (Fig. 1b) might be responsible.

However the bivariate polar plots (Fig. 7) indicate that high SO_2 concentration tended to occur under high speed wind from the south and southeast directions, which shifted relative to the locations of the SO_2 point sources (Fig. 1b). The reason might be geographical since the position (North) of the Bukhan Mountain block the wind and rather promotes the circulation of air masses. Similar trends were observed in a previous study (Heo et al., 2009).

The decrease of both sulfate and SO_2 concentrations between 10:00 – 17:00 (Fig. 6b) could be due to the dilution effect from rising BL height. Since fSO_4 showed only minor increases between 12:00 – 17:00 when RH was low (Fig. 6c), gas phase photochemical production of sulfate during daytime was unlikely to be an important process. This observation, together with the nighttime increase of sulfate associated with high RH, suggests that aqueous phase processing is an important driver for sulfate formation in Seoul during wintertime. This conclusion is consistent with previous studies which found that aqueous phase reactions were an important pathway for sulfate formation in the atmosphere under humid conditions (Ervens et al., 2011;Ge et al., 2012b).

In this study, as mentioned in the earlier section, nitrate, sulfate and chloride in PM_1 appeared to be fully neutralized by ammonium, indicating that the inorganic species were mainly present in the forms of NH_4NO_3, $(NH_4)_2SO_4$ and NH_4Cl. Since nitrate was more abundant compared to sulfate and chloride (Fig. 4a), the ammonium diurnal pattern was similar to that of nitrate. However, a gradual increase of ammonium during nighttime was observed, likely due to the enhancement of the sulfate concentration. Chloride accounted for a small fraction of the PM_1 mass and displayed a morning rush hour peak, suggesting that the source of chloride is probably local, such as vehicle emissions. Indeed, the polar plot of chloride in Fig. 7 does show the feature of local source since high concentration occurred mostly at slow wind speed. Further, chloride showed a similar diurnal pattern as HOA (Section 3.3, Fig. 10) and good correlation with HOA (r =0.8; Table 2).

In contrast to ammonium and nitrate, OA concentration tended to remain high overnight and started to increase in the morning with a maximum usually occurring at 8:00 (Fig. 5a). This morning increase was likely the outcome of shallow BL coupled with enhanced primary emissions from rush-hour traffic. Further discussions on this are given in section 3.3.

3.2 Size distributions of the main components of PM_1

The average mass-based size distributions of AMS species in terms of vacuum aerodynamic diameter (D_{va}, (DeCarlo et al., 2004)) are shown in Fig. 4c. Nitrate and sulfate had relatively different size distribution profiles with the mode of sulfate being about 100 nm larger than the

mode of nitrate. A possible reason for this difference was likely that nitrate was mainly formed through photochemical reactions whereas sulfate was more likely to be formed by aqueous-phase reactions during this study. Another reason was that sulfate was overall more aged than nitrate. As discussed in previous sections, sulfate in Seoul was likely to be transported from regional sources during nighttime whereas nitrate was apparently formed mostly locally. The daily variations in the nitrate and sulfate size distributions (Figs. 5b, c, Fig. S4) further support the different formation processes for these two compounds. The size distributions of sulfate showed a prevalent droplet accumulation mode (D_{va} = 500 nm) that stayed fairly constant compared to the one of nitrate (Fig. S4). However, the size distributions of nitrate became broader between 9:00 and 15:00 with significant changes in concentrations (Fig. 5c, Fig. S4a)). In addition, nitrate size distribution was quite broad (Figs. 4c, d), similar to observations in various urban locations. (e.g., Sun et al., 2009;Sun et al., 2011a;Drewnick et al., 2004;Salcedo et al., 2006;Weimer et al., 2006;Young et al., 2016;Zhang et al., 2005b)

The average size distribution of OA was wider than those of the inorganic species, peaking at a D_{va} of ~ 400 nm (Fig. 4c). The OA size distribution varied as a function of the time of day (Fig. 5a), with a broader profile extending to D_{va} < 100 nm observed during the morning rush hour and night time when primary emission are dominant. The wide size distribution of organics reflected the contribution made by both primary and secondary aerosols, i.e., the fine mode from primary aerosols and the accumulation mode from secondary formation. Similar observations were reported from China, (e.g., Huang et al., 2010;Sun et al., 2010) and some urban areas in North America (Aiken et al., 2009;Alfarra et al., 2004;Drewnick et al., 2004;Ge et al., 2012b;Zhang et al., 2005b) and Europe (Allan et al., 2003;Dall'Osto et al., 2013).

3.3 OA characteristics and source apportionment

3.3.1 Bulk composition and elemental ratios of OA

Atmospheric OA are composed of complex materials that originate from different sources and have undergone different atmospheric processes. Understanding the chemical composition and sources of OA is important for understanding the impacts of these aerosols.

Overall, OA from Seoul during wintertime was found to be composed of approximately 71% carbon, 18% oxygen, 9% hydrogen, and 2% nitrogen (Fig. 4e). The average carbon-normalized molecular formula of OA was $C_1H_{1.8}O_{0.37}N_{0.022}S_{0.0009}$, yielding an average organic mass-to-carbon

ratio (OM/OC) of 1.67. The largest component of the OA mass spectral signal was found to be the $C_xH_y^+$ ion family (57%, Fig. 4e), followed by the $C_xH_yO_1^+$ (25%) and $C_xH_yO_2^+$ (11%) ion families, with smaller contributions from the $C_xH_yN_p^+$ (4%), $C_xH_yN_pO_z^+$ (2%), and $H_yO_1^+$ (1%) ion families. The largest peak in the average OA spectrum was at *m/z* = 43 (Fig. 4f), accounting for 8% of the total OA signal with a composition of $C_2H_3O^+$ (49%), $C_3H_7^+$ (49%), $CHON^+$ (1%), and $C_2H_5N^+$ (1%). The second largest peak (6% of the total OA signal) in the average OA spectrum was at *m/z* = 44, which was dominated by the CO_2^+ ion (86.7%) followed by $C_2H_4O^+$ (7.8 %), $C_2H_6N^+$ (2.7%), CH_2NO^+ (2.6%) and $C_3H_8^+$ (0.2%). The peak at *m/z* = 60 was composed almost entirely of $C_2H_4O_2^+$ (94%) and 88% of the peak at *m/z* = 73 was composed of $C_3H_5O_2^+$, both of which are the tracers of wood burning (Aiken et al., 2008;Alfarra et al., 2007). The peak at *m/z* = 57, which is used as a tracer for hydrocarbon like organics from vehicle emissions (Zhang et al., 2005a) accounted for 4% of the total OA signal, and was composed predominantly of $C_4H_9^+$ (75%) and $C_3H_5O^+$ (22%) in this study.

The time series of the H/C, O/C, N/C and S/C ratios of OA are shown in Figs. 3e and f. The O/C ratio of an OA indicates its average oxidation level and more aged and oxidized organics tend to have higher O/C ratios (Aiken et al., 2008;Jimenez et al., 2009). The O/C varied substantially during this study ranging from 0.05 to 0.63 and the average O/C ratio was 0.37±0.09. The average H/C ratio was 1.79±0.07 (1.60 – 2.29) and the average OM/OC was 1.67±0.12 (1.26 – 2.03). These values, which were calculated using the updated elemental analysis method (Canagaratna et al., 2015), are within the range of revised values observed at other urban locations (Canagaratna et al., 2015 and references within). Upon examining the diurnal patterns, we also found that the O/C and OM/OC ratios started to increase in the morning and peaked in the afternoon (Figs. 8a and e). The lowest value of both parameters occurred at around 8:00, due to enhanced vehicle emissions during morning rush hours coupled with low BL height, which was also evident in the diurnal profile of the H/C ratio (Fig. 8b). However, during daytime (8:00 – 16:00), O/C ratio generally increased and H/C ratio decreased suggesting that SOA production or mixing with more aged aerosol from regional sources was important during daytime and outweighed the emissions POA. The decrease of the OM/OC and O/C ratios as well as the increase of H/C ratio in the late evening (19:00－20:00) were consistent with an enhancement of POA emissions during the evening rush hour and dinner time.

Although organic ions containing nitrogen and sulfur had relatively low abundance (average N/C = 0.018; average S/C = 0.001), both nitrogen-to-carbon (N/C) and sulfur-to-carbon (S/C) ratios showed distinct diurnal profiles where N/C enhanced during daytime (8:00 – 16:00) and increased again from late evening (19:00), suggesting that particulate nitrogen-containing compounds in Seoul were probably from both primary emissions and secondary formation. However, S/C showed relatively strong enhancement during daytime (8:00 – 16:00), suggesting that sulfur containing organics were mainly formed by secondary processes during daytime. This is further confirmed by considering the correlation between different OA factors vs. AMS spectral ions; nitrogen containing ions had good correlation both with POA and SOA factors whereas sulfur containing ions had good correlation only with OOAs (Fig. S5; see section 3.3.2).

3.3.2 Organic aerosol source apportionment and characteristics of OA factors

Separation of distinct organic aerosol sources can be achieved through the application of multivariate models, such as PMF (Lanz et al., 2007;Ulbrich et al., 2009;Zhang et al., 2011). In this study, five OA factors were determined, consisting of three POA factors (HOA, COA and BBOA) and two SOA factors (LV-OOA and SV-OOA). The O/C ratios for the factors were: LV-OOA = 0.68; SV-OOA = 0.56; BBOA = 0.34; COA = 0.14; and HOA = 0.06. The elemental ratios of the factors were estimated using the updated method reported by Canagaratna et al. (2015). A comparison of the O/C and H/C ratio of each PMF factor, as determined by the methods of Aiken et al. (2008) and Canagaratna et al. (2015), can be found in Table S1. An overview of the chemical composition and temporal variations of the five factors is shown in Figs. 9, 10 and Fig. S7. The five factors made similar contributions to total OA mass, with LV-OOA (26%) representing the largest fraction of the OA mass and the smallest faction accounted for by SV-OOA (15%). BBOA, COA and HOA accounted for 23, 20 and 16% of the total OA mass, respectively. Together, primary components on average accounted for 59% of the total OA mass and SOA accounted for 41% (Fig. 10k). The chemical composition and temporal variations of each factor are discussed in detail below.

3.3.2.1 Hydrocarbon-like OA (HOA)

Alkyl fragments ($C_nH_{2n+1}^+$ and $C_nH_{2n-1}^+$) made a substantial contribution to the HOA factor, with major peaks at *m/z*'s 41, 43, 55, and 57 which were mostly composed of $C_3H_5^+$, $C_3H_7^+$, $C_4H_7^+$, and $C_4H_9^+$ ions, respectively (Fig. 10a). These major peaks and the overall picket fence fragmentation

pattern resulting from the $C_nH_{2n+1}^+$ ions are typical features of the HOA spectra reported in other studies and are due to the association of these aerosols with fossil fuel combustion (e.g.,Alfarra et al., 2007;Lanz et al., 2008;Sun et al., 2011b;Zhang et al., 2005a;Huang et al., 2010;Morgan et al., 2010;Ng et al., 2011). In addition, strong correlations were observed between the time series of HOA and the $C_nH_{2n+1}^+$ and $C_nH_{2n-1}^+$ ions, e.g., $C_3H_7^+$ (r = 0.91), $C_4H_7^+$ (r = 0.85), $C_4H_9^+$ (r = 0.95), and $C_5H_{11}^+$ (r = 0.96) (Fig. 9a and Table 2). Due to the dominance of chemically reduced hydrocarbon species, the O/C ratio of the HOA in this study was low (0.06), whereas the H/C ratio was high (2.21). The O/C ratio of HOA of this study was similar to the updated values of HOA (0.05 − 0.25) from other studies (Canagaratna et al., 2015).

The regular enhancement of HOA around 7:00 − 9:00, as shown in its diurnal profile (Fig. 10f), was consistent with the occurrence of morning rush hour traffic in Seoul and the association of HOA with vehicle emissions. HOA concentration decreased rapidly from 8:00 to 12:00 noon and remained low in the afternoon, mainly due to dilution associated with rising of BL height. A slow increase of HOA concentration began at ~16:00 and persisted till the next morning, suggesting that the shallow BL enhanced the gradual accumulation of the pollutants from vehicle emissions. However, the correlations of the time series of HOA with gaseous tracers of primary emissions (i.e., BC, NO_2, and CO), were only moderate (Fig. 9a and Table 2), mainly because these pollutants are emitted not only from vehicular sources, but also from other combustion sources, e.g., biomass burning. Indeed, the correlations are much stronger between these pollutants and total POA (= HOA + COA + BBOA) (r = 0.7 – 0.81; Fig. 11 and Table 2).

In this study, major differences were observed between weekdays and weekends for HOA including other primary species, e.g., BC and POA factors (Fig. S10). For example, the diurnal pattern of HOA and BC changed significantly between the weekdays and weekends, a general decrease in the morning rush hour peak over the weekend was observed, likely due to a decrease in commuting activities because people were more likely to be at home. This weekend effect is a typical urban features which were observed in Fresno (Young et al., 2016) and Northeastern U.S. (Zhou et al., 2016b), as well.

3.3.2.2 Cooking OA (COA)

COA, as resolved by AMS OA spectra, has been widely reported in urban areas with high population densities (He et al., 2010;Huang et al., 2010;Mohr et al., 2012;Sun et al., 2011b;Young et al., 2016;Ge et al., 2012a;Wang et al., 2016;Xu et al., 2014); however no results have yet been

reported from Seoul. In this study, COA was found to account for 20% of the total OA mass, higher than HOA (Fig. 10k). The diurnal pattern of COA displayed a large evening peak, with a maximum concentration occurring at 19:00, i.e., dinner time. Elevated COA concentration and larger fractional contribution to OA mass were observed throughout the night (Figs. 10g, l).

Similar to HOA, the mass spectrum of COA in this study also contained many alkyl fragments, but to a lesser extent (75.8 % of the total signal in COA spectrum compared to 87.9% of the total signal in HOA spectrum) (Fig. 10b). However, COA contains significantly larger amounts of oxygen-containing ions than HOA (e.g., $C_xH_yO_1^+$ = 15.4% vs. 7.6% and $C_xH_yO_2^+$ = 5.1% vs. 2.3%) (Fig. 10a), and thus had a higher O/C ratio (0.14) and a lower H/C ratio (1.89). The OM/OC ratio was 1.3 and the H/C ratio is 1.78 for COA. The observed O/C ratio (0.14) of COA in Seoul was at the lower end of the range (0.14-0.27) of the revised measured O/C ratio of COA in other studies, e.g., Barcelona (0.27) (Mohr et al., 2012), New York City (NYC) (0.23) (Sun et al., 2011a) and Fresno (0.14 in 2010 (Ge et al., 2012b) and 0.19 in 2013 (Young et al., 2016)). Previous studies suggest that $C_3H_3O^+$ (*m/z* 55) and $C_3H_5O^+$ (*m/z* 57) were major fragments of aliphatic acids (e.g., linoleic acid and palmitic acid) in cooking oils or animal fat and therefore used these ions as key tracers for identifying the presence of aerosols from cooking related activities (He et al., 2004;Adhikary et al., 2010;Mohr et al., 2009;Zhao et al., 2007). In addition, $C_5H_8O^+$ (*m/z* 84) and $C_6H_{10}O^+$ (*m/z* 98) have been proposed as AMS tracers for COA as well (Ge et al., 2012a;Sun et al., 2011b). In this study, the time series of COA correlated well with these ions, e.g., $C_3H_3O^+$ (r = 0.86), $C_5H_8O^+$ (r = 0.93), $C_7H_{12}O^+$ (r = 0.89), and $C_6H_{10}O^+$ (r = 0.95) (Fig. 9b and Table 2) and COA was a major contributor to the signals of $C_5H_8O^+$, $C_6H_{10}O^+$, and $C_7H_{12}O^+$, accounting for 57%, 69%, and 52%, respectively, of their signals (Fig. S6). To show the chemical difference between COA and other OA factors, Mohr et al. (2012) used the relationships between the fractions of OA signals at m/z 55 and m/z 57 (i.e., *f*55 and *f*57) or between those of $C_3H_3O^+$ and $C_3H_5O^+$ (i.e., $fC_3H_3O^+$ and $fC_3H_5O^+$) after subtracting the contributions from the oxygenated OA factors and found that the ratios between m/z 55 ($C_4H_7^+$ + $C_3H_3O^+$) and *m/z* 57 ($C_4H_9^+$ + $C_3H_5O^+$) in COA were much higher (2.2 − 2.8) than the ratios (0.9-1.1) in other POAs (e.g., HOA and BBOA). The COA resolved in Seoul in this study had an *m/z* 55 to *m/z* 57 ratio of 2.2, within the range of the values for COA reported in Mohr et al. (2012) (Fig. S9). In addition, the ratios between *f*55 and *f*57 for OA in Seoul increased proportionally as the fractional contribution of COA to total OA increased (Fig. S9b), with a "V" shape indicated by the two edges defined by the COA and

the HOA factors from several urban AMS data sets (Mohr et al., 2012). These observations together confirm the identification of COA at Seoul.

3.3.2.3 Biomass burning OA (BBOA)

Wood combustion was found to be another important POA source (23 %, Fig.10k) in Seoul during winter, in addition to vehicle and cooking emissions. BBOA is typically prevalent during winter in locations where wood is used for residential heating (Ge et al., 2012a;Crippa et al., 2013;Zhang et al., 2015;Young et al., 2016). The mass spectrum of BBOA showed strong signals of oxygenated ions ($C_xH_yO_1^+$: 27.1% of total BBOA signal and $C_xH_yO_2^+$: 10.6 % of total BBOA signal) and was more oxidized than HOA and COA (Fig. 10). Among the three POA factors, the O/C ratio of BBOA was the highest (0.34) and the H/C ratio was the lowest (1.74), similar to the results reported in several previous studies (e.g., Aiken et al., 2009;Ge et al., 2012a;Mohr et al., 2012). An analysis of the OA spectra (Fig. 10c) revealed the typical features of BBOA, with dominant peaks at *m/z* 60 (100% being $C_2H_4O_2^+$) and *m/z* 73 (95% being $C_3H_5O_2^+$), which are known fragments of levoglucosan and related species (e.g., mannosan and galactosan) (Cubison et al., 2011). Scatter plots of *f*44 versus *f*60 indicate a higher *f*60 and lower *f*44 (i.e., toward the center of the triangle area of the biomass burning plumes) as the relative importance of BBOA to the total OA increased (Fig. S9). The *f*44 and *f*60 of BBOA (0.05 vs. 0.016) in this study were also within the range of values found for the other ambient BBOA factors or biomass burning aerosols from chamber studies. HOA and COA, in contrast, had much lower *f*60 values (< 0.01). The time series of BBOA correlated well with $C_2H_4O_2^+$ (r = 0.85) and $C_3H_5O_2^+$ (r =0.74) (Fig. 9d and Table 2) as well as other biomass burning tracer species, including potassium (r = 0.63) and BC (r = 0.82). BBOA also correlated well with nitrogen-containing species, particularly $C_3H_4N^+$ (r = 0.75), $C_2H_4N^+$ (r = 0.70) and CHN^+ (r = 0.58), which was consistent with the emissions of nitriles from biomass burning activities (Simoneit et al., 2003). There was also a strong correlation between the concentration of polycyclic aromatic hydrocarbons (PAHs; r = 0.90) and BBOA, indicating that biomass burning was a main source of PAH in Seoul during wintertime. Similarly, it was found in Fresno, California, during wintertime that BBOA correlates well with N-containing ions and PAHs (Ge et al., 2012a;Young et al., 2016). Given that PAHs are byproducts of incomplete combustion, many of which are mutagenic and carcinogenic (Dzepina et al., 2007;Hannigan et al., 1998;Marr et al., 2006), our findings suggest that adverse health effects associated with biomass burning emissions should be of concern during winter in the Seoul region.

BBOA was the most abundant primary OA in Seoul during this study, account for 39% of the POA mass and 23% of the total OA mass. However biomass burning is not the main fuel for the residential heating in Seoul and thus, the BBOA observed in this study must have originated from other wood burning activities, either locally or regionally. The fact that the observed BBOA was relatively oxidized (O/C=0.34), with a large contribution from *m/z* 44 (*f*44 = 5.1%), was consistent with the observations of more aged BBOA instead of primary woodstove emissions (Crippa et al., 2013;Zhang et al., 2015;Zhou et al., 2016a). The diurnal profile of BBOA showed an enhancement at around 9:00 and a background BBOA concentration of ~ 1 μg/m^3. Given that the polar plot of BBOA showed high concentrations at both low and high wind speeds (Fig. 7), the sources of BBOA in Seoul likely include both local and regional wood burning activities. Local wood burning activities were possibly for the purposes of heating open and public areas (e.g., construction areas, market), dispose of leaves and woody trash in the city, and heating some residences. Regional sources of BBOA are possibly from open biomass burning in agricultural area near Seoul (Heo et al., 2009) and transport from North Korea or further from Russia (Jung et al., 2016).

3.3.2.4. Semi-volatile and low volatile oxygenated OA (SV-OOA and LV-OOA)

In addition to the three POA factors, two OOA factors were identified and were found to account for an average of 41% of the OA mass (Fig. 10k). OOA is ubiquitous and dominant in the atmosphere (Jimenez et al., 2009;Zhang et al., 2007a) but usually accounts for less than half of the OA mass observed in urban locations during winter such as NYC, Tokyo, Fresno and Manchester (Zhang et al., 2007b).

In many cases, OOA can be further separated into a low volatile/more oxygenated OOA (LV-OOA/MO-OOA) and a semi-volatile/less oxygenated OOA (SV-OOA/LO-OOA), which represent different degrees of aging and oxidation (Jimenez et al., 2009;Ng et al., 2010, and reference therein;Setyan et al., 2012;Xu et al., 2015). In this study, two OOA factors, SV-OOA and LV-OOA were observed to account for 15 and 26% of the total OA mass, respectively (Fig. 10k). As shown in the triangle plots in Fig. S9, SV-OOA (O/C = 0.56; H/C = 1.90) resides within the region representing fresher SOA, with a low *f*44, and LV-OOA (O/C = 0.68; H/C = 1.61) was similar to aged and highly oxidized OA, with a high *f*44. It has been observed that fresh OOA becomes increasingly more oxidized and less volatile through aging processes in the atmosphere resulting in LV-OOA and that the evolution of SOA is regarded as a continuum of oxidation. The mass

spectra of both LV-OOA and SV-OOA were very similar to the spectra of OOA factors reported in other cities (e.g., Hayes et al., 2013;Mohr et al., 2012;Zhang et al., 2014).

Comparisons between the time series of SV-OOA and LV-OOA with gaseous species, aerosol species, and meteorological parameters further confirmed their secondary nature. As shown in Table 2, SV-OOA and LV-OOA strongly correlated with nitrate (r = 0.87 and 0.63, respectively) and sulfate (r = 0.71 and 0.80, respectively), whereas the correlations between POA factors and the inorganic aerosol species were low (r = 0.09 – 0.41). The Pearson's correlation coefficient between total OOA (= SV-OOA + LV-OOA) and the sum of secondary inorganic aerosols (NO_3^- + SO_4^{2-} + NH_4^+) was as high as 0.91 (Fig. 11a). These results confirm the association of SV-OOA and LV-OOA with SOA.

As discussed above, sulfate in Seoul is mainly associated with regional sources, while nitrate is often formed more locally due to the intense urban emissions of NO_x. The better correlations between SV-OOA and nitrate and between LV-OOA and sulfate (Table 2) suggest that SV-OOA likely had more local sources whereas LV-OOA likely had more regional sources. Furthermore, SV-OOA correlated more strongly with methanesulfonic acid (MSA), an SOA species that tends to be semi-volatile. As shown in Table 2, the correlations of SV-OOA and LV-OOA with AMS spectral ions for MSA (Ge et al., 2012a), i.e., $CH_3SO_2^+$ (r = 0.90 and 0.53, respectively) and $CH_2SO_2^+$ (r = 0.83 and 0.53, respectively) corroborated the different natures of SV-OOA (fresher, more local) and LV-OOA (aged, more regional). The diurnal profiles of SV-OOA and LV-OOA also reflected the features of local versus regional sources (Figs. 10 i,j). SV-OOA concentration had a clear peak during mid-morning to afternoon (10:00-11:00, Fig. 10i); however, LV-OOA concentration was relatively constant throughout the day, suggesting regional sources of this aerosol component (Fig. 10j). Similar observations were also reported in other areas such as North America (e.g., Budisulistiorini et al., 2015;Sun et al., 2011b;Woody et al., 2016;Zhou et al., 2016b;Zhang et al., 2005b), Europe (e.g., Mohr et al., 2012;Young et al., 2015), and Asia (e.g., Huang et al., 2010;Jiang et al., 2015;Wang et al., 2016). Finally, the polar plots of both OOAs showed more dispersed features compared to the POA factors, especially HOA and COA, but SV-OOA appeared to have a stronger association with local processes, as its high concentrations tended to be associated with lower wind speed, compared to LV-OOA (Fig. 7).

3.4 Relative Importance of local and regional influences on air quality in Seoul during winter

In an effort to improve ambient air quality, the Korean government enacted "Special Act on Seoul Metropolitan Air Quality Improvement" to regulate the concentrations of key pollutants such as SO_2, CO, NO_2, O_3, PM, and Pb (lead) in 2005. However, till today, Seoul is still facing poor air quality problems, especially in terms of high concentrations of $PM_{2.5}$ and O_3. $PM_{2.5}$ has been one of the primary concerns due to its detrimental impacts on human health as well as on visibility. O_3 is an important air pollutant itself and can contribute to the secondary formation of $PM_{2.5}$. Since the development of effective air pollution control policies must rely on knowledge about the sources, it is important to investigate the major formation processes and emission sources that contribute to the high PM loadings. Therefore, in this section, we examine how both primary emissions and secondary formation affect PM loadings in Seoul during winter.

Fig. 12 shows comparisons of the average concentrations of PM_1 components as well as other air pollutants under high and low PM loading conditions depicted on Figs. 2 and 3. The average concentrations of all aerosol components and OA sources were 1.7 – 8.6 times higher during the high loading periods compared to the low loading periods (Table 3, Figs. 12e,f). A main reason appeared to be meteorological conditions. For example, high loading periods were generally stagnant with low wind speed (0.99 ± 0.7 m/s) (Figs. 12a, b), leading to the accumulation of pollutants, especially those mainly from local sources. Indeed, among all species, SV-OOA, HOA, nitrate, and COA showed the highest increases during high loading periods and their average enhancement in concentrations were 8.6, 5.2, 4.7 and 4.5 times, respectively, of the values during the low loading periods (Fig. 12e). In addition to accumulate primary pollutants, stable meteorology condition can also lead to longer atmospheric residence time, which facilitates the local formation of secondary species such as SV-OOA and nitrate. Furthermore, the relatively high RH during the high loading periods (71% ± 15; Table 3, Fig. 12a) likely also enhanced the formation of secondary species such as sulfate and LV-OOA through aqueous-phase processing. A further evidence for enhanced aqueous-phase processing of secondary aerosol species during high PM loading periods is shown in Fig. 13; the size distributions of all secondary inorganic species (nitrate, sulfate and ammonium) were significantly larger during the more polluted periods, peaking at 500-600 nm in D_{va}, compared to the cleaner periods (peaking at 300-400 nm). A previous study in a US city during winter time also observed that high RH conditions, thus

enhanced aqueous-phase processing, led to increases in the size modes of sulfate, nitrate, and ammonium (Ge et al., 2012b).

The enhancement ratios of the other primary pollutants such as CO, SO_2, NO_2, BC, and BBOA, were in the range of 1.2 – 2.5, significantly lower than those of HOA and COA (Fig. 12e), reflecting the facts that they all had bigger contributions from regional sources compared to HOA and COA (Fig. 7). Average O_3 concentration, on the other hand, showed a substantial decrease (by ~ 70%) during high aerosol loading periods (Fig. 12e and 12f). In addition to enhanced titration reactions by NO_x, another possible reason for O_3 decrease was reduced photochemical reactions due to inhibition of light by high concentration of PM (He et al., 2014).

The high loading periods corresponded closely to air masses that are classified as cluster 4 (Fig. 14), which had the shorted trajectories, i.e., slowest wind speeds, as well as the lowest travel height compared to the other three clusters. The air mass in cluster 4 thus likely held larger amounts of pollutants and precursors from the ground. In addition, since air masses in each cluster were expected to have passed over regions indicated by the corresponding trajectories, investigating the composition and masses of aerosol in each cluster can shed lights on how various upwind areas influence air quality at the measurement site. For example, PM in this type of air masses (cluster 4) could also be more oxidized, containing a larger fraction of secondary pollutants, due to longer residence time in the atmosphere, therefore was composed of a higher fraction of nitrate.

The average aerosol composition during the high loading periods (Fig. 12) was similar to that for the whole period (Fig. 4), consistent with frequent occurrence of high aerosol pollution episodes and indicate that these events determined the overall characteristics of PM_1 in Seoul during winter. Given that local emissions were mostly responsible for these pollution events, controlling the emissions of both primary aerosol particles and precursors for secondary species from local sources might be an effective way to manage air quality in Seoul during winter time.

Low PM loading periods (average $\pm 1\sigma = 12.6 \pm 7.1$ μg m^{-3} for PM_1) were commonly associated with high WS (1.8 ± 1.1 m/s), low RH (50 %), and long distance transport of air masses from Russia, Northern China (such as Inner Mongolia), Mongolia or North Korea (i.e., Cluster 1,2 and 3 from back trajectory analysis; Fig. 14). All three Clusters appeared to originate from Russia, however there were some differences among clusters. For example, cluster 1 passed over Mongolia and North Korea whereas Clusters 2 and 3 passed over China. Furthermore Cluster 3 was composed of the longest trajectories.

Aerosol composition was somewhat different between the high loading and low the loading periods. Since strong wind could inhibit the accumulation of local primary and secondary species while bring in pollutants from upwind sources, the mass fractions of species influenced more strongly by local sources, such as nitrate (27 vs 20 %), SV-OOA (8 vs 3 %), HOA (7 vs 4 %), and COA (8 vs 7 %) were lower during low loading periods compared to more polluted periods, whereas those of regional sources such as sulfate (10 vs 12 %), LV-OOA (10 vs 20 %), BBOA (9 vs 12 %) enhanced (Fig. 12). Although Clusters 1, 2 and 3 all represented regional transport conditions, PM mass concentrations and compositions were somewhat different because of different origin of air masses. Specifically, Cluster 1 and 2 were almost directly to the north whereas Cluster 3 was more towards the west (Fig. 14). In comparison, Cluster 1 and 2 had higher fractions of BBOA but a lower fraction of LV-OOA and sulfate. A possible explanation for this observation is that northwest area might have more anthropogenic sources than the north area does.

As shown in Fig. 2, PM concentration often changed abruptly with the appearance and dissipation of a high PM_1 event occurring rather quickly (within several hours). The changes were commonly associated with changes in meteorological conditions, especially wind direction and speed. Similar trends of sudden changes in air quality have also been observed in other studies in China, and have been attributed to meteorology (Zhang et al., 2015). For these reasons, it appears that regional meteorology played an important role in causing high PM pollution conditions in Seoul.

4 Conclusions

Aerosol composition, size distribution, sources, and evolution processes were investigated using an HR-ToF-AMS and an SMPS in Seoul, Korea, during winter 2015. The average PM_1 concentration was 27.5 μg m^{-3} and the total mass was dominated by organics (44%), followed by nitrate (24%) and sulfate (10%). Secondary materials (i.e., NO_3^-, SO_4^{2-}, NH_4^+, SV-OOA and LV-OOA) together accounted for 64% of the PM_1 total mass, with the remainder being primary materials (HOA, COA, BBOA and BC). Cooking, fossil fuel combustion, and wood combustion were identified as major POA sources in Seoul, contributing an average 59% of total OA mass during this study.

Meteorological conditions and various emission sources influenced the concentrations, compositions, size distributions, and properties of aerosol particles in Seoul. High PM pollution

periods tended to build up over a period of 4-5 days and were interleaved with multiple days of relatively clean periods. High aerosol loading periods were commonly found under relatively stagnant conditions with low wind speed and aerosol from these periods was characterized with enhanced fractional contributions of nitrate (27%) and SV-OOA (8%), indicating a strong influence from local production of secondary aerosol. In contrast, under relatively dynamic meteorological conditions with higher wind speed, aerosol loading was generally low and PM_1 contained larger fractions of species with regional sources, such as sulfate (12%), LV-OOA (20%), and BBOA (12%). The average O/C ratio of OA was also higher during low loading periods (0.41 vs. 0.35 for high loading periods), indicating the influence of more oxidized OA likely from long range transport.

Total POA concentration was enhanced by three times during high loading periods. In addition, an enhancement of the fractional contributions of BBOA from the high loading periods (9%) was observed during low loading periods (12%). In this study, we found that nearly half of the OA mass was POA and that PAHs in PM_1 were mainly from biomass burning ($r = 0.90$). These results suggest that it is important to reduce emissions from combustion sources to improve air quality and protect public health in Seoul during wintertime. Together, local formation of secondary species (e.g., Nitrate, SV-OOA) during stable meteorological conditions was also significant for high PM loadings. Thus, the serious pollution observed in Seoul during winter was caused by combination of factors, including meteorological conditions, emission by local primary sources, secondary formation as well as transport of air masses from upwind locations and other unknown factors.

Acknowledgments

This work was supported by the Korea Institute of Science and Technology (KIST). QZ acknowledges the Changjiang Scholars program of the Chinese Ministry of Education.

References

Adhikary, B., Carmichael, G. R., Kulkarni, S., Wei, C., Tang, Y., D'Allura, A., Mena-Carrasco, M., Streets, D. G., Zhang, Q., Pierce, R. B., Al-Saadi, J. A., Emmons, L. K., Pfister, G. G., Avery, M. A., Barrick, J. D., Blake, D. R., Brune, W. H., Cohen, R. C., Dibb, J. E., Fried, A.,

Heikes, B. G., Huey, L. G., O'Sullivan, D. W., Sachse, G. W., Shetter, R. E., Singh, H. B., Campos, T. L., Cantrell, C. A., Flocke, F. M., Dunlea, E. J., Jimenez, J. L., Weinheimer, A. J., Crounse, J. D., Wennberg, P. O., Schauer, J. J., Stone, E. A., Jaffe, D. A., and Reidmiller, D. R.: A regional scale modeling analysis of aerosol and trace gas distributions over the eastern Pacific during the INTEX-B field campaign, Atmospheric Chemistry and Physics, 10, 2091-2115, 2010.

Aiken, A. C., Decarlo, P. F., Kroll, J. H., Worsnop, D. R., Huffman, J. A., Docherty, K. S., Ulbrich, I. M., Mohr, C., Kimmel, J. R., Sueper, D., Sun, Y., Zhang, Q., Trimborn, A., Northway, M., Ziemann, P. J., Canagaratna, M. R., Onasch, T. B., Alfarra, M. R., Prevot, A. S. H., Dommen, J., Duplissy, J., Metzger, A., Baltensperger, U., and Jimenez, J. L.: O/C and OM/OC ratios of primary, secondary, and ambient organic aerosols with high-resolution time-of-flight aerosol mass spectrometry, Environmental Science & Technology, 42, 4478-4485, 10.1021/es703009q, 2008.

Aiken, A. C., Salcedo, D., Cubison, M. J., Huffman, J. A., DeCarlo, P. F., Ulbrich, I. M., Docherty, K. S., Sueper, D., Kimmel, J. R., Worsnop, D. R., Trimborn, A., Northway, M., Stone, E. A., Schauer, J. J., Volkamer, R. M., Fortner, E., de Foy, B., Wang, J., Laskin, A., Shutthanandan, V., Zheng, J., Zhang, R., Gaffney, J., Marley, N. A., Paredes-Miranda, G., Arnott, W. P., Molina, L. T., Sosa, G., and Jimenez, J. L.: Mexico City aerosol analysis during MILAGRO using high resolution aerosol mass spectrometry at the urban supersite (T0) – Part 1: Fine particle composition and organic source apportionment, Atmospheric Chemistry and Physics, 9, 6633-6653, 10.5194/acp-9-6633-2009, 2009.

Alfarra, M. R., Coe, H., Allan, J. D., Bower, K. N., Boudries, H., Canagaratna, M. R., Jimenez, J. L., Jayne, J. T., Garforth, A., Li, S.-M., and Worsnop, D. R.: Characterization of urban and ruralorganic particulate in the Lower Fraser Valley using two Aerodyne Aerosol Mass Spectrometers, Atmospheric Environment, 38, 13, 2004.

Alfarra, M. R., Prevot, A. S. H., Szidat, S., Sandradewi, J., Weimer, S., Lanz, V. A., Schreiber, D., Mohr, M., and Baltensperger, U.: Identification of the Mass Spectral Signature of Organic Aerosols from Wood Burning Emissions, Environmental Science & Technology, 41, 5770-5777, 10.1021/es062289b, 2007.

Allan, J. D., Alfarra, M. R., Bower, K. N., Williams, P. I., Gallagher, M. W., Jimenez, J. L., McDonald, A. G., Nemitz, E., Canagaratna, M. R., Jayne, J. T., Coe, H., and Worsnop, D. R.: Quantitative sampling using an Aerodyne aerosol mass spectrometer - 2. Measurements of fine particulate chemical composition in two U.K. cities, Journal of Geophysical Research-Atmospheres, 108, 10.1029/2002jd002359, 2003.

Allan, J. D., Delia, A. E., Coe, H., Bower, K. N., Alfarra, M. R., Jimenez, J. L., Middlebrook, A. M., Drewnick, F., Onasch, T. B., Canagaratna, M. R., Jayne, J. T., and Worsnop, D. R.: A generalised method for the extraction of chemically resolved mass spectra from aerodyne aerosol mass spectrometer data, J Aerosol Sci, 35, 909-922, 10.1016/j.jaerosci.2004.02.007, 2004.

Brown, S. G., Roberts, P. T., McCarthy, M. C., Lurmann, F. W., and Hyslop, N. P.: Wintertime vertical variations in particulate matter (PM) and precursor concentrations in the San Joaquin Valley during the California Regional coarse PM/fine PM Air Quality Study, Journal of the Air & Waste Management Association, 56, 1267-1277, 2006.

Budisulistiorini, S. H., Li, X., Bairai, S. T., Renfro, J., Liu, Y., Liu, Y. J., McKinney, K. A., Martin, S. T., McNeill, V. F., Pye, H. O. T., Nenes, A., Neff, M. E., Stone, E. A., Mueller, S., Knote, C., Shaw, S. L., Zhang, Z., Gold, A., and Surratt, J. D.: Examining the effects of anthropogenic emissions on isoprene-derived secondary organic aerosol formation during the 2013 Southern Oxidant and Aerosol Study (SOAS) at the Look Rock, Tennessee ground site, Atmospheric Chemistry and Physics, 15, 8871-8888, 10.5194/acp-15-8871-2015, 2015.

Canagaratna, M. R., Jayne, J. T., Jimenez, J. L., Allan, J. D., Alfarra, M. R., Zhang, Q., Onasch, T. B., Drewnick, F., Coe, H., Middlebrook, A., Delia, A., Williams, L. R., Trimborn, A. M., Northway, M. J., DeCarlo, P. F., Kolb, C. E., Davidovits, P., and Worsnop, D. R.: Chemical and microphysical characterization of ambient aerosols with the aerodyne aerosol mass spectrometer, Mass Spectrometry Reviews, 26, 185-222, 10.1002/mas.20115, 2007.

Canagaratna, M. R., Jimenez, J. L., Kroll, J. H., Chen, Q., Kessler, S. H., Massoli, P., Hildebrandt Ruiz, L., Fortner, E., Williams, L. R., Wilson, K. R., Surratt, J. D., Donahue, N. M., Jayne, J. T., and Worsnop, D. R.: Elemental ratio measurements of organic compounds using aerosol mass spectrometry: characterization, improved calibration, and implications, Atmospheric Chemistry and Physics, 15, 253-272, 10.5194/acp-15-253-2015, 2015.

Cao, J.-j., Wang, Q.-y., Chow, J. C., Watson, J. G., Tie, X.-x., Shen, Z.-x., Wang, P., and An, Z.-s.: Impacts of aerosol compositions on visibility impairment in Xi'an, China, Atmospheric Environment, 59, 559-566, 10.1016/j.atmosenv.2012.05.036, 2012.

Choi, J.-K., Heo, J.-B., Ban, S.-J., Yi, S.-M., and Zoh, K.-D.: Chemical characteristics of $PM_{2.5}$ aerosol in Incheon, Korea, Atmospheric Environment, 60, 583-592, 2012.

Choi, N. R., Lee, S. P., Lee, J. Y., Jung, C. H., and Kim, Y. P.: Speciation and source identification of organic compounds in PM10 over Seoul, South Korea, Chemosphere, 144, 1589-1596, 10.1016/j.chemosphere.2015.10.041, 2016.

Crippa, M., DeCarlo, P. F., Slowik, J. G., Mohr, C., Heringa, M. F., Chirico, R., Poulain, L., Freutel, F., Sciare, J., Cozic, J., Di Marco, C. F., Elsasser, M., Nicolas, J. B., Marchand, N., Abidi, E., Wiedensohler, A., Drewnick, F., Schneider, J., Borrmann, S., Nemitz, E., Zimmermann, R., Jaffrezo, J. L., Prevot, A. S. H., and Baltensperger, U.: Wintertime aerosol chemical composition and source apportionment of the organic fraction in the metropolitan area of Paris, Atmospheric Chemistry and Physics, 13, 961-981, 10.5194/acp-13-961-2013, 2013.

Cubison, M. J., Ortega, A. M., Hayes, P. L., Farmer, D. K., Day, D., Lechner, M. J., Brune, W. H., Apel, E., Diskin, G. S., Fisher, J. A., Fuelberg, H. E., Hecobian, A., Knapp, D. J., Mikoviny, T., Riemer, D., Sachse, G. W., Sessions, W., Weber, R. J., Weinheimer, A. J., Wisthaler, A., and Jimenez, J. L.: Effects of aging on organic aerosol from open biomass burning smoke in aircraft and laboratory studies, Atmospheric Chemistry and Physics, 11, 12049-12064, 10.5194/acp-11-12049-2011, 2011.

Dall'Osto, M., Ovadnevaite, J., Ceburnis, D., Martin, D., Healy, R. M., O'Connor, I. P., Kourtchev, I., Sodeau, J. R., Wenger, J. C., and O'Dowd, C.: Characterization of urban aerosol in Cork city (Ireland) using aerosol mass spectrometry, Atmospheric Chemistry and Physics, 13, 4997-5015, 10.5194/acp-13-4997-2013, 2013.

DeCarlo, P. F., Slowik, J. G., Worsnop, D. R., Davidovits, P., and Jimenez, J. L.: Particle morphology and density characterization by combined mobility and aerodynamic diameter

measurements. Part 1: Theory, Aerosol Science and Technology, 38, 1185-1205, Doi 10.1080/02786820590928897, 2004.

DeCarlo, P. F., Kimmel, J. R., Trimborn, A., Northway, M. J., Jayne, J. T., Aiken, A. C., Gonin, M., Fuhrer, K., Horvath, T., Docherty, K. S., Worsnop, D. R., and Jimenez, J. L.: Field-deployable, high-resolution, time-of-flight aerosol mass spectrometer, Analytical Chemistry, 78, 8281-8289, 10.1021/ac061249n, 2006.

Ding, A. J., Fu, C. B., Yang, X. Q., Sun, J. N., Zheng, L. F., Xie, Y. N., Herrmann, E., Nie, W., Petaja, T., Kerminen, V. M., and Kulmala, M.: Ozone and fine particle in the western Yangtze River Delta: an overview of 1 yr data at the SORPES station, Atmospheric Chemistry and Physics, 13, 5813-5830, 10.5194/acp-13-5813-2013, 2013.

Ding, A. J., Huang, X., Nie, W., Sun, J. N., Kerminen, V. M., Petäjä, T., Su, H., Cheng, Y. F., Yang, X. Q., Wang, M. H., Chi, X. G., Wang, J. P., Virkkula, A., Guo, W. D., Yuan, J., Wang, S. Y., Zhang, R. J., Wu, Y. F., Song, Y., Zhu, T., Zilitinkevich, S., Kulmala, M., and Fu, C. B.: Enhanced haze pollution by black carbon in megacities in China, Geophysical Research Letters, 43, 2873-2879, 10.1002/2016gl067745, 2016.

Draxler, R. R., Stunder, B., Rolph, G., Stein, A., and Taylor, A.: HYSPLIT_4 User's Guide, available at http://www.arl.noaa.gov/documents/reports/hysplit_user_guide.pdf, NOAA Air Resources Laboratory, Silver Spring,Maryland, USA

2012.

Draxler, R. R. a. H., G. D.: Description of the HYSPLIT_4 modeling system, available at: http://www.arl.noaa.gov/documents/reports/arl-224.pdf (last access: 5 January 2014),NOAA Air Resources Laboratory, Silver Spring, Maryland,USA, 1997.

Drewnick, F., Jayne, J. T., Canagaratna, M., Worsnop, D. R., and Demerjian, K. L.: Measurement of ambient aerosol composition during the PMTACS-NY 2001 using an aerosol mass spectrometer. Part II: Chemically speciated mass distributions, Aerosol Science and Technology, 38, 104-117, 10.1080/02786820390229534, 2004.

Dzepina, K., Arey, J., Marr, L. C., Worsnop, D. R., Salcedo, D., Zhang, Q., Onasch, T. B., Molina, L. T., Molina, M. J., and Jimenez, J. L.: Detection of particle-phase polycyclic aromatic hydrocarbons in Mexico City using an aerosol mass spectrometer, Int J Mass Spectrom, 263, 152-170, http://dx.doi.org/10.1016/j.ijms.2007.01.010, 2007.

Ervens, B., Turpin, B. J., and Weber, R. J.: Secondary organic aerosol formation in cloud droplets and aqueous particles (aqSOA): a review of laboratory, field and model studies, Atmospheric Chemistry and Physics, 11, 11069-11102, 10.5194/acp-11-11069-2011, 2011.

Ge, X., Setyan, A., Sun, Y., and Zhang, Q.: Primary and secondary organic aerosols in Fresno, California during wintertime: Results from high resolution aerosol mass spectrometry, Journal of Geophysical Research-Atmospheres, 117, 10.1029/2012jd018026, 2012a.

Ge, X. L., Zhang, Q., Sun, Y. L., Ruehl, C. R., and Setyan, A.: Effect of aqueous-phase processing on aerosol chemistry and size distributions in Fresno, California, during wintertime, Environ. Chem., 9, 221-235, 10.1071/en11168, 2012b.

Gelencsér, A., May, B., Simpson, D., Sánchez-Ochoa, A., Kasper-Giebl, A., Puxbaum, H., Caseiro, A., Pio, C., and Legrand, M.: Source apportionment of PM2.5 organic aerosol over Europe: Primary/secondary, natural/anthropogenic, and fossil/biogenic origin, - 112, 2007.

Guo, S., Hu, M., Zamora, M. L., Peng, J., Shang, D., Zheng, J., Du, Z., Wu, Z., Shao, M., Zeng, L., Molina, M. J., and Zhang, R.: Elucidating severe urban haze formation in China, Proceedings of the National Academy of Sciences, 111, 17373-17378, 10.1073/pnas.1419604111, 2014.

Hannigan, M. P., Cass, G. R., Penman, B. W., Crespi, C. L., Lafleur, A. L., Busby, W. F., Thilly, W. G., and Simoneit, B. R. T.: Bioassay-Directed Chemical Analysis of Los Angeles Airborne Particulate Matter Using a Human Cell Mutagenicity Assay, Environ Sci Technol, 32, 3502-3514, 10.1021/es9706561, 1998.

Harrison, R. M., and Yin, J.: Particulate matter in the atmosphere: which particle properties are important for its effects on health?, Science of the Total Environment, 249, 85-101, http://dx.doi.org/10.1016/S0048-9697(99)00513-6, 2000.

Hayes, P. L., Ortega, A. M., Cubison, M. J., Froyd, K. D., Zhao, Y., Cliff, S. S., Hu, W. W., Toohey, D. W., Flynn, J. H., Lefer, B. L., Grossberg, N., Alvarez, S., Rappenglueck, B., Taylor, J. W., Allan, J. D., Holloway, J. S., Gilman, J. B., Kuster, W. C., De Gouw, J. A., Massoli, P., Zhang, X., Liu, J., Weber, R. J., Corrigan, A. L., Russell, L. M., Isaacman, G., Worton, D. R., Kreisberg, N. M., Goldstein, A. H., Thalman, R., Waxman, E. M., Volkamer, R., Lin, Y. H., Surratt, J. D., Kleindienst, T. E., Offenberg, J. H., Dusanter, S., Griffith, S., Stevens, P. S., Brioude, J., Angevine, W. M., and Jimenez, J. L.: Organic aerosol composition and sources in Pasadena, California, during the 2010 CalNex campaign, Journal of Geophysical Research-Atmospheres, 118, 9233-9257, 10.1002/jgrd.50530, 2013.

He, H., Wang, Y. S., Ma, Q. X., Ma, J. Z., Chu, B. W., Ji, D. S., Tang, G. Q., Liu, C., Zhang, H. X., and Hao, J. M.: Mineral dust and NOx promote the conversion of SO2 to sulfate in heavy pollution days, Scientific Reports, 4, 10.1038/srep04172, 2014.

He, J., Zielinska, B., and Balasubramanian, R.: Composition of semi-volatile organic compounds in the urban atmosphere of Singapore: influence of biomass burning, Atmospheric Chemistry and Physics, 10, 11401-11413, 10.5194/acp-10-11401-2010, 2010.

He, L.-Y., Huang, X.-F., Xue, L., Hu, M., Lin, Y., Zheng, J., Zhang, R., and Zhang, Y.-H.: Submicron aerosol analysis and organic source apportionment in an urban atmosphere in Pearl River Delta of China using high-resolution aerosol mass spectrometry, Journal of Geophysical Research-Atmospheres, 116, 10.1029/2010jd014566, 2011.

He, L. Y., Hu, M., Huang, X. F., Yu, B. D., Zhang, Y. H., and Liu, D. Q.: Measurement of emissions of fine particulate organic matter from Chinese cooking, Atmospheric Environment, 38, 6557-6564, 10.1016/j.atmosenv.2004.08.034, 2004.

Hennigan, C. J., Bergin, M. H., Russell, A. G., Nenes, A., and Weber, R. J.: Gas/particle partitioning of water-soluble organic aerosol in Atlanta, Atmospheric Chemistry and Physics, 9, 3613-3628, 10.5194/acp-9-3613-2009, 2009.

Heo, J. B., Hopke, P. K., and Yi, S. M.: Source apportionment of PM2.5 in Seoul, Korea, Atmospheric Chemistry and Physics, 9, 4957-4971, 2009.

Huang, R.-J., Zhang, Y., Bozzetti, C., Ho, K.-F., Cao, J.-J., Han, Y., Daellenbach, K. R., Slowik, J. G., Platt, S. M., Canonaco, F., Zotter, P., Wolf, R., Pieber, S. M., Bruns, E. A., Crippa, M.,

Ciarelli, G., Piazzalunga, A., Schwikowski, M., Abbaszade, G., Schnelle-Kreis, J., Zimmermann, R., An, Z., Szidat, S., Baltensperger, U., El Haddad, I., and Prevot, A. S. H.: High secondary aerosol contribution to particulate pollution during haze events in China, Nature, 514, 218-222, 10.1038/nature13774, 2014.

Huang, X. F., He, L. Y., Hu, M., Canagaratna, M. R., Sun, Y., Zhang, Q., Zhu, T., Xue, L., Zeng, L. W., Liu, X. G., Zhang, Y. H., Jayne, J. T., Ng, N. L., and Worsnop, D. R.: Highly time-resolved chemical characterization of atmospheric submicron particles during 2008 Beijing Olympic Games using an Aerodyne High-Resolution Aerosol Mass Spectrometer, Atmospheric Chemistry and Physics, 10, 8933-8945, 10.5194/acp-10-8933-2010, 2010.

Huang, X. F., He, L. Y., Hu, M., Canagaratna, M. R., Kroll, J. H., Ng, N. L., Zhang, Y. H., Lin, Y., Xue, L., Sun, T. L., Liu, X. G., Shao, M., Jayne, J. T., and Worsnop, D. R.: Characterization of submicron aerosols at a rural site in Pearl River Delta of China using an Aerodyne High-Resolution Aerosol Mass Spectrometer, Atmospheric Chemistry and Physics, 11, 1865-1877, 10.5194/acp-11-1865-2011, 2011.

Huang, X. F., He, L. Y., Xue, L., Sun, T. L., Zeng, L. W., Gong, Z. H., Hu, M., and Zhu, T.: Highly time-resolved chemical characterization of atmospheric fine particles during 2010 Shanghai World Expo, Atmospheric Chemistry and Physics, 12, 4897-4907, 10.5194/acp-12-4897-2012, 2012.

IPCC: Summary for policymakers, in: Climate Change 2013: The Physical Science Basis. Contribution of Working Group 1 to the Fifth Assessment Report of the Intergovernmental Panel on Climate Change, edited by: Stocker, T. F., Qin, D., Plattner, G.-K., Tignor, M., Allen, S. K., Boschung, J., Nauels, A., Xia, Y., Bex, V., and Midgley, P. M., Cambridge University Press, Cambridge, UK, New York, NY, USA, 3-29, 2013.

Jiang, Q., Sun, Y. L., Wang, Z., and Yin, Y.: Aerosol composition and sources during the Chinese Spring Festival: fireworks, secondary aerosol, and holiday effects, Atmospheric Chemistry and Physics, 15, 6023-6034, 10.5194/acp-15-6023-2015, 2015.

Jimenez, J. L., Canagaratna, M. R., Donahue, N. M., Prevot, A. S. H., Zhang, Q., Kroll, J. H., DeCarlo, P. F., Allan, J. D., Coe, H., Ng, N. L., Aiken, A. C., Docherty, K. S., Ulbrich, I. M., Grieshop, A. P., Robinson, A. L., Duplissy, J., Smith, J. D., Wilson, K. R., Lanz, V. A., Hueglin, C., Sun, Y. L., Tian, J., Laaksonen, A., Raatikainen, T., Rautiainen, J., Vaattovaara, P., Ehn, M., Kulmala, M., Tomlinson, J. M., Collins, D. R., Cubison, M. J., Dunlea, E. J., Huffman, J. A., Onasch, T. B., Alfarra, M. R., Williams, P. I., Bower, K., Kondo, Y., Schneider, J., Drewnick, F., Borrmann, S., Weimer, S., Demerjian, K., Salcedo, D., Cottrell, L., Griffin, R., Takami, A., Miyoshi, T., Hatakeyama, S., Shimono, A., Sun, J. Y., Zhang, Y. M., Dzepina, K., Kimmel, J. R., Sueper, D., Jayne, J. T., Herndon, S. C., Trimborn, A. M., Williams, L. R., Wood, E. C., Middlebrook, A. M., Kolb, C. E., Baltensperger, U., and Worsnop, D. R.: Evolution of Organic Aerosols in the Atmosphere, Science, 326, 1525-1529, 10.1126/science.1180353, 2009.

Jung, J., Lyu, Y., Lee, M., Hwang, T., Lee, S., and Oh, S.: Impact of Siberian forest fires on the atmosphere over the Korean Peninsula during summer 2014, Atmospheric Chemistry and Physics, 16, 6757-6770, 10.5194/acp-16-6757-2016, 2016.

Kaneyasu, N., Ohta, S., and Murao, N.: SEASONAL-VARIATION IN THE CHEMICAL-COMPOSITION OF ATMOSPHERIC AEROSOLS AND GASEOUS SPECIES IN

SAPPORO, JAPAN, Atmospheric Environment, 29, 1559-1568, 10.1016/1352-2310(94)00356-p, 1995.

Kang, S. H., Heo, J., Oh, I. Y., Kim, J., Lim, W. H., Cho, Y., Choi, E. K., Yi, S. M., Do Shin, S., Kim, H., and Oh, S.: Ambient air pollution and out-of-hospital cardiac arrest, Int. J. Cardiol., 203, 1086-1092, 10.1016/j.ijcard.2015.11.100, 2016.

Kim, E., Hopke, P. K., and Edgerton, E. S.: Source identification of Atlanta aerosol by positive matrix factorization, Journal of the Air & Waste Management Association, 53, 731-739, 2003.

Kim, Y., Yoon, S. C., Kim, S. W., Kim, K. Y., Lim, H. C., and Ryu, J.: Observation of new particle formation and growth events in Asian continental outflow, Atmospheric Environment, 64, 160-168, 10.1016/j.atmosenv.2012.09.057, 2013.

Kim, Y., Kim, S.-W., Yoon, S.-C., Kim, M.-H., and Park, K.-H.: Aerosol properties and associated regional meteorology during winter pollution event at Gosan climate observatory, Korea, Atmospheric Environment, 85, 9-17, 10.1016/j.atmosenv.2013.11.041, 2014.

KOSAE: Studies of Measures for Improving/Complementing the Master Plan for the Metropolitan Air Quality Management. Report to the Korean Ministry of Environment (in Korean), Gwacheon, Korea. , 2009.

Kulmala, M., Lappalainen, H. K., Petaja, T., Kurten, T., Kerminen, V. M., Viisanen, Y., Hari, P., Sorvari, S., Back, J., Bondur, V., Kasimov, N., Kotlyakov, V., Matvienko, G., Baklanov, A., Guo, H. D., Ding, A., Hansson, H. C., and Zilitinkevich, S.: Introduction: The Pan-Eurasian Experiment (PEEX) - multidisciplinary, multiscale and multicomponent research and capacity-building initiative, Atmospheric Chemistry and Physics, 15, 13085-13096, 10.5194/acp-15-13085-2015, 2015.

Kuwata, M., Zorn, S. R., and Martin, S. T.: Using Elemental Ratios to Predict the Density of Organic Material Composed of Carbon, Hydrogen, and Oxygen, Environmental Science & Technology, 46, 787-794, 10.1021/es202525q, 2012.

Lanz, V. A., Alfarra, M. R., Baltensperger, U., Buchmann, B., Hueglin, C., and Prevot, A. S. H.: Source apportionment of submicron organic aerosols at an urban site by factor analytical modelling of aerosol mass spectra, Atmospheric Chemistry and Physics, 7, 1503-1522, 2007.

Lanz, V. A., Alfarra, M. R., Baltensperger, U., Buchmann, B., Hueglin, C., Szidat, S., Wehrli, M. N., Wacker, L., Weimer, S., Caseiro, A., Puxbaum, H., and Prevot, A. S. H.: Source Attribution of Submicron Organic Aerosols during Wintertime Inversions by Advanced Factor Analysis of Aerosol Mass Spectra, Environmental Science & Technology, 42, 214-220, 10.1021/es0707207, 2008.

Li, Y. J., Lee, B. P., Su, L., Fung, J. C. H., and Chan, C. K.: Seasonal characteristics of fine particulate matter (PM) based on high-resolution time-of-flight aerosol mass spectrometric (HR-ToF-AMS) measurements at the HKUST Supersite in Hong Kong, Atmos. Chem. Phys., 15, 37-53, 10.5194/acp-15-37-2015, 2015.

Lim, S., Lee, M., Lee, G., Kim, S., Yoon, S., and Kang, K.: Ionic and carbonaceous compositions of PM10, PM2.5 and PM1.0 at Gosan ABC Superstation and their ratios as source signature, Atmospheric Chemistry and Physics, 12, 2007-2024, 10.5194/acp-12-2007-2012, 2012.

Liu, X. G., Li, J., Qu, Y., Han, T., Hou, L., Gu, J., Chen, C., Yang, Y., Liu, X., Yang, T., Zhang, Y., Tian, H., and Hu, M.: Formation and evolution mechanism of regional haze: a case study in the megacity Beijing, China, Atmospheric Chemistry and Physics, 13, 4501-4514, 10.5194/acp-13-4501-2013, 2013.

Lurmann, F. W., Brown, S. G., McCarthy, M. C., and Roberts, P. T.: Processes Influencing Secondary Aerosol Formation in the San Joaquin Valley during Winter, Journal of the Air & Waste Management Association (1995), 56, 1679-1693, 2006.

Marr, L. C., Dzepina, K., Jimenez, J. L., Reisen, F., Bethel, H. L., Arey, J., Gaffney, J. S., Marley, N. A., Molina, L. T., and Molina, M. J.: Sources and transformations of particle-bound polycyclic aromatic hydrocarbons in Mexico City, Atmos. Chem. Phys., 6, 1733-1745, 10.5194/acp-6-1733-2006, 2006.

Middlebrook, A. M., Bahreini, R., Jimenez, J. L., and Canagaratna, M. R.: Evaluation of Composition-Dependent Collection Efficiencies for the Aerodyne Aerosol Mass Spectrometer using Field Data, Aerosol Science and Technology, 46, 258-271, 10.1080/02786826.2011.620041, 2012.

Mohr, C., Huffman, J. A., Cubison, M. J., Aiken, A. C., Docherty, K. S., Kimmel, J. R., Ulbrich, I. M., Hannigan, M., and Jimenez, J. L.: Characterization of Primary Organic Aerosol Emissions from Meat Cooking, Trash Burning, and Motor Vehicles with High-Resolution Aerosol Mass Spectrometry and Comparison with Ambient and Chamber Observations, Environmental Science & Technology, 43, 2443-2449, Doi 10.1021/Es8011518, 2009.

Mohr, C., DeCarlo, P. F., Heringa, M. F., Chirico, R., Slowik, J. G., Richter, R., Reche, C., Alastuey, A., Querol, X., Seco, R., Penuelas, J., Jimenez, J. L., Crippa, M., Zimmermann, R., Baltensperger, U., and Prevot, A. S. H.: Identification and quantification of organic aerosol from cooking and other sources in Barcelona using aerosol mass spectrometer data, Atmospheric Chemistry and Physics, 12, 1649-1665, 10.5194/acp-12-1649-2012, 2012.

Morgan, W. T., Allan, J. D., Bower, K. N., Highwood, E. J., Liu, D., McMeeking, G. R., Northway, M. J., Williams, P. I., Krejci, R., and Coe, H.: Airborne measurements of the spatial distribution of aerosol chemical composition across Europe and evolution of the organic fraction, Atmospheric Chemistry and Physics, 10, 4065-4083, 10.5194/acp-10-4065-2010, 2010.

Ng, N. L., Canagaratna, M. R., Zhang, Q., Jimenez, J. L., Tian, J., Ulbrich, I. M., Kroll, J. H., Docherty, K. S., Chhabra, P. S., Bahreini, R., Murphy, S. M., Seinfeld, J. H., Hildebrandt, L., Donahue, N. M., DeCarlo, P. F., Lanz, V. A., Prevot, A. S. H., Dinar, E., Rudich, Y., and Worsnop, D. R.: Organic aerosol components observed in Northern Hemispheric datasets from Aerosol Mass Spectrometry, Atmospheric Chemistry and Physics, 10, 4625-4641, 10.5194/acp-10-4625-2010, 2010.

Ng, N. L., Canagaratna, M. R., Jimenez, J. L., Zhang, Q., Ulbrich, I. M., and Worsnop, D. R.: Real-Time Methods for Estimating Organic Component Mass Concentrations from Aerosol Mass Spectrometer Data, Environmental Science & Technology, 45, 910-916, Doi 10.1021/Es102951k, 2011.

NIER: Annual report of air quality in Korea 2013. Available at: http://webbook.me.go.kr/DLi-File/NIER/09/019/5584427.pdf 2014. (21/01/2016), 2014.

Paatero, P., and Tapper, U.: Positive matrix factorization - A nonnegative factor model with optimal utilization of error-Estimates of data values, Environmetrics, 5, 111-126, 10.1002/env.3170050203, 1994.

Parworth, C., Fast, J., Mei, F., Shippert, T., Sivaraman, C., Tilp, A., Watson, T., and Zhang, Q.: Long-term measurements of submicrometer aerosol chemistry at the southern great plains (SPG) using an aerosol chemical speciation monitor (ACSM), Atmospheric Environment, 106, 12, 10.1016/j.atmosenv.2015.01.060, 2015.

Petaja, T., Jarvi, L., Kerminen, V. M., Ding, A. J., Sun, J. N., Nie, W., Kujansuu, J., Virkkula, A., Yang, X. Q., Fu, C. B., Zilitinkevich, S., and Kulmala, M.: Enhanced air pollution via aerosol-boundary layer feedback in China, Sci Rep, 6, 18998, 10.1038/srep18998, 2016.

Pope III, C. A., and Dockery, D. W.: Health Effects of Fine Particulate Air Pollution: Lines that Connect, Journal of the Air & Waste Management Association, 56, 709-742, 2006.

Pöschl, U.: Atmospheric Aerosols: Composition, Transformation, Climate and Health Effects, Angewandte Chemie International Edition, 44, 7520-7540, 10.1002/anie.200501122, 2005.

Quan, J., Zhang, Q., He, H., Liu, J., Huang, M., and Jin, H.: Analysis of the formation of fog and haze in North China Plain (NCP), Atmospheric Chemistry and Physics, 11, 8205-8214, 10.5194/acp-11-8205-2011, 2011.

Salcedo, D., Onasch, T. B., Dzepina, K., Canagaratna, M. R., Zhang, Q., Huffman, J. A., DeCarlo, P. F., Jayne, J. T., Mortimer, P., Worsnop, D. R., Kolb, C. E., Johnson, K. S., Zuberi, B., Marr, L. C., Volkamer, R., Molina, L. T., Molina, M. J., Cardenas, B., Bernabe, R. M., Marquez, C., Gaffney, J. S., Marley, N. A., Laskin, A., Shutthanandan, V., Xie, Y., Brune, W., Lesher, R., Shirley, T., and Jimenez, J. L.: Characterization of ambient aerosols in Mexico City during the MCMA-2003 campaign with Aerosol Mass Spectrometry: results from the CENICA Supersite, Atmospheric Chemistry and Physics, 6, 925-946, 2006.

Seinfeld, J. H., and Pandis, S. N.: Atmospheric Chemistry and Physics: From Air Pollution to Climate Change, 2nd ed., John Wiley & Sons, New York, 1232 pp., 2006.

Setyan, A., Zhang, Q., Merkel, M., Knighton, W. B., Sun, Y., Song, C., Shilling, J. E., Onasch, T. B., Herndon, S. C., Worsnop, D. R., Fast, J. D., Zaveri, R. A., Berg, L. K., Wiedensohler, A., Flowers, B. A., Dubey, M. K., and Subramanian, R.: Characterization of submicron particles influenced by mixed biogenic and anthropogenic emissions using high-resolution aerosol mass spectrometry: results from CARES, Atmospheric Chemistry and Physics, 12, 8131-8156, 10.5194/acp-12-8131-2012, 2012.

Simoneit, B. R. T., Rushdi, A. I., bin Abas, M. R., and Didyk, B. M.: Alkyl Amides and Nitriles as Novel Tracers for Biomass Burning, Environmental Science & Technology, 37, 16-21, 10.1021/es020811y, 2003.

Sun, J., Zhang, Q., Canagaratna, M. R., Zhang, Y., Ng, N. L., Sun, Y., Jayne, J. T., Zhang, X., Zhang, X., and Worsnop, D. R.: Highly time- and size-resolved characterization of submicron aerosol particles in Beijing using an Aerodyne Aerosol Mass Spectrometer, Atmospheric Environment, 44, 131-140, 10.1016/j.atmosenv.2009.03.020, 2010.

Sun, Y., Zhang, Q., Macdonald, A. M., Hayden, K., Li, S. M., Liggio, J., Liu, P. S. K., Anlauf, K. G., Leaitch, W. R., Steffen, A., Cubison, M., Worsnop, D. R., van Donkelaar, A., and Martin, R. V.: Size-resolved aerosol chemistry on Whistler Mountain, Canada with a high-resolution

aerosol mass spectrometer during INTEX-B, Atmospheric Chemistry and Physics, 9, 3095-3111, 2009.

Sun, Y., Wang, Z., Dong, H., Yang, T., Li, J., Pan, X., Chen, P., and Jayne, J. T.: Characterization of summer organic and inorganic aerosols in Beijing, China with an Aerosol Chemical Speciation Monitor, Atmospheric Environment, 51, 250-259, 10.1016/j.atmosenv.2012.01.013, 2012.

Sun, Y., Jiang, Q., Wang, Z., Fu, P., Li, J., Yang, T., and Yin, Y.: Investigation of the sources and evolution processes of severe haze pollution in Beijing in January 2013, Journal of Geophysical Research-Atmospheres, 119, 4380-4398, 10.1002/2014jd021641, 2014.

Sun, Y. L., Zhang, Q., Schwab, J. J., Chen, W. N., Bae, M. S., Lin, Y. C., Hung, H. M., and Demerjian, K. L.: A case study of aerosol processing and evolution in summer in New York City, Atmos. Chem. Phys., 11, 12737-12750, 10.5194/acp-11-12737-2011, 2011a.

Sun, Y. L., Zhang, Q., Schwab, J. J., Demerjian, K. L., Chen, W. N., Bae, M. S., Hung, H. M., Hogrefe, O., Frank, B., Rattigan, O. V., and Lin, Y. C.: Characterization of the sources and processes of organic and inorganic aerosols in New York city with a high-resolution time-of-flight aerosol mass apectrometer, Atmospheric Chemistry and Physics, 11, 1581-1602, 10.5194/acp-11-1581-2011, 2011b.

Ulbrich, I. M., Canagaratna, M. R., Zhang, Q., Worsnop, D. R., and Jimenez, J. L.: Interpretation of organic components from Positive Matrix Factorization of aerosol mass spectrometric data, Atmospheric Chemistry and Physics, 9, 2891-2918, 10.5194/acp-9-2891-2009, 2009.

Wang, J., Ge, X., Chen, Y., Shen, Y., Zhang, Q., Sun, Y., Xu, J., Ge, S., Yu, H., and Chen, M.: Highly time-resolved urban aerosol characteristics during springtime in Yangtze River Delta, China: insights from soot particle aerosol mass spectrometry, Atmos. Chem. Phys., 16, 9109-9127, 10.5194/acp-16-9109-2016, 2016.

Weimer, S., Drewnick, F., Hogrefe, O., Schwab, J. J., Rhoads, K., Orsini, D., Canagaratna, M., Worsnop, D. R., and Demerjian, K. L.: Size-selective nonrefractory ambient aerosol measurements during the Particulate Matter Technology Assessment and Characterization Study - New York 2004 Winter Intensive in New York City, Journal of Geophysical Research-Atmospheres, 111, 17, 10.1029/2006jd007215, 2006.

Woody, M. C., Baker, K. R., Hayes, P. L., Jimenez, J. L., Koo, B., and Pye, H. O. T.: Understanding sources of organic aerosol during CalNex-2010 using the CMAQ-VBS, Atmospheric Chemistry and Physics, 16, 4081-4100, 10.5194/acp-16-4081-2016, 2016.

Xu, J., Zhang, Q., Chen, M., Ge, X., Ren, J., and Qin, D.: Chemical composition, sources, and processes of urban aerosols during summertime in northwest China: insights from high-resolution aerosol mass spectrometry, Atmospheric Chemistry and Physics, 14, 12593-12611, 10.5194/acp-14-12593-2014, 2014.

Xu, J., Shi, J., Zhang, Q., Ge, X., Canonaco, F., Prévôt, A. S. H., Vonwiller, M., Szidat, S., Ge, J., Ma, J., An, Y., Kang, S., and Qin, D.: Wintertime organic and inorganic aerosols in Lanzhou, China: Sources, processes and comparison with the results during summer, Atmospheric Chemistry and Physics Discussions, 1-52, 10.5194/acp-2016-278, 2016.

Xu, L., Guo, H., Boyd, C. M., Klein, M., Bougiatioti, A., Cerully, K. M., Hite, J. R., Isaacman-VanWertz, G., Kreisberg, N. M., Knote, C., Olson, K., Koss, A., Goldstein, A. H., Hering, S.

V., de Gouw, J., Baumann, K., Lee, S.-H., Nenes, A., Weber, R. J., and Ng, N. L.: Effects of anthropogenic emissions on aerosol formation from isoprene and monoterpenes in the southeastern United States, Proceedings of the National Academy of Sciences of the United States of America, 112, 37-42, 10.1073/pnas.1417609112, 2015.

Young, D. E., Allan, J. D., Williams, P. I., Green, D. C., Flynn, M. J., Harrison, R. M., Yin, J., Gallagher, M. W., and Coe, H.: Investigating the annual behaviour of submicron secondary inorganic and organic aerosols in London, Atmospheric Chemistry and Physics, 15, 6351-6366, 10.5194/acp-15-6351-2015, 2015.

Young, D. E., Kim, H., Parworth, C., Zhou, S., Zhang, X., Cappa, C. D., Seco, R., Kim, S., and Zhang, Q.: Influences of emission sources and meteorology on aerosol chemistry in a polluted urban environment: results from DISCOVER-AQ California, Atmos. Chem. Phys., 16, 5427-5451, 10.5194/acp-16-5427-2016, 2016.

Zhang, J. K., Sun, Y., Liu, Z. R., Ji, D. S., Hu, B., Liu, Q., and Wang, Y. S.: Characterization of submicron aerosols during a month of serious pollution in Beijing, 2013, Atmospheric Chemistry and Physics, 14, 2887-2903, 10.5194/acp-14-2887-2014, 2014.

Zhang, Q., Alfarra, M. R., Worsnop, D. R., Allan, J. D., Coe, H., Canagaratna, M. R., and Jimenez, J. L.: Deconvolution and quantification of hydrocarbon-like and oxygenated organic aerosols based on aerosol mass spectrometry, Environmental Science & Technology, 39, 4938-4952, 10.1021/Es048568l, 2005a.

Zhang, Q., Canagaratna, M. R., Jayne, J. T., Worsnop, D. R., and Jimenez, J. L.: Time- and size-resolved chemical composition of submicron particles in Pittsburgh: Implications for aerosol sources and processes, Journal of Geophysical Research-Atmospheres, 110, 10.1029/2004jd004649, 2005b.

Zhang, Q., Jimenez, J. L., Canagaratna, M. R., Allan, J. D., Coe, H., Ulbrich, I., Alfarra, M. R., Takami, A., Middlebrook, A. M., Sun, Y. L., Dzepina, K., Dunlea, E., Docherty, K., DeCarlo, P. F., Salcedo, D., Onasch, T., Jayne, J. T., Miyoshi, T., Shimono, A., Hatakeyama, S., Takegawa, N., Kondo, Y., Schneider, J., Drewnick, F., Borrmann, S., Weimer, S., Demerjian, K., Williams, P., Bower, K., Bahreini, R., Cottrell, L., Griffin, R. J., Rautiainen, J., Sun, J. Y., Zhang, Y. M., and Worsnop, D. R.: Ubiquity and dominance of oxygenated species in organic aerosols in anthropogenically-influenced Northern Hemisphere midlatitudes, Geophysical Research Letters, 34, L13801, Artn L13801, Doi 10.1029/2007gl029979, 2007a.

Zhang, Q., Jimenez, J. L., Worsnop, D. R., and Canagaratna, M.: A case study of urban particle acidity and its influence on secondary organic aerosol, Environmental Science & Technology, 41, 3213-3219, 10.1021/Es061812j, 2007b.

Zhang, Q., Jimenez, J. L., Canagaratna, M. R., Ulbrich, I. M., Ng, N. L., Worsnop, D. R., and Sun, Y.: Understanding atmospheric organic aerosols via factor analysis of aerosol mass spectrometry: a review, Analytical and bioanalytical chemistry, 401, 3045-3067, 10.1007/s00216-011-5355-y, 2011.

Zhang, Y. J., Tang, L. L., Wang, Z., Yu, H. X., Sun, Y. L., Liu, D., Qin, W., Canonaco, F., Prevot, A. S. H., Zhang, H. L., and Zhou, H. C.: Insights into characteristics, sources, and evolution of submicron aerosols during harvest seasons in the Yangtze River delta region, China, Atmospheric Chemistry and Physics, 15, 1331-1349, 10.5194/acp-15-1331-2015, 2015.

Zhao, Y., Hu, M., Slanina, S., and Zhang, Y.: Chemical compositions of fine particulate organic matter emitted from Chinese cooking, Environmental Science & Technology, 41, 99-105, 10.1021/es0614518, 2007.

Zhou, S., Collier, S., Jaffe, D. A., Briggs, N. L., Hee, J., Sedlacek Iii, A. J., Kleinman, L., Onasch, T. B., and Zhang, Q.: Regional Influence of Wildfires on Aerosol Chemistry in the Western US and Insights into Atmospheric Aging of Biomass Burning Organic Aerosol, Atmos. Chem. Phys. Discuss., 2016, 1-27, 10.5194/acp-2016-823, 2016a.

Zhou, S., Collier, S., Xu, J. Z., Mei, F., Wang, J., Lee, Y. N., Sedlacek, A. J., Springston, S. R., Sun, Y. L., and Zhang, Q.: Influences of upwind emission sources and atmospheric processing on aerosol chemistry and properties at a rural location in the Northeastern US, Journal of Geophysical Research-Atmospheres, 121, 6049-6065, 10.1002/2015jd024568, 2016b.

Tables

Table 1. Average (± 1 standard deviation), minimum and maximum concentrations of the particulate matter (PM_1) species and the total PM_1 mass over the whole campaign, and the average contribution of each of the PM_1 species to the total PM_1 mass.

	Average conc. ± one standard deviation (μg m^{-3})	Minimum conc. (μg m^{-3})	Maximum conc. (μg m^{-3})	Fraction of total PM_1 (%)	Detection limit (3min/ 6min) (μg m^{-3})
Organics	12.1 ± 8.03	1.32	53.1	44	0.03/0.02
Nitrate	6.55 ± 5.12	0.18	26.0	24	0.01/0.01
Sulfate	2.87 ± 2.00	0.38	10.7	10	0.01/0.01
Ammonium	3.11 ± 2.20	0.21	10.5	12	0.02/0.01
Chloride	0.26 ± 0.32	0	2.91	1	0.01/0.01
Black carbon	2.54 ± 1.66	0	10.1	9	0.1/0.05
Total PM_1	27.5 ± 17.2	1.32	90.7	-	0.04/0.03

Table 2. Correlation coefficient (Pearson's r) for the linear regressions between organic aerosol (OA) factors (including the sum of primary factors (primary OA (POA) = hydrocarbon like OA (HOA) + cooking OA (COA) + biomass burning OA (BBOA)), as well as the sum of the oxidized factors (oxidized OA (OOA) = semi-volatile OOA (SV-OOA) + low volatile (LV-OOA)), and various particle- and gas-phase species, and ions.

r	HOA	COA	BBOA	POA (HOA+ COA+BBOA)	SV-OOA	LV-OOA	OOA (SV-OOA+ LV-OOA)
Nitrate	0.32	0.30	0.41	0.43	**0.87**	0.63	**0.87**
Sulfate	0.25	0.17	0.09	0.23	**0.71**	**0.80**	**0.88**
Ammonium	0.41	0.30	0.37	0.45	**0.87**	0.69	**0.90**
Chloride	**0.80**	0.30	0.50	0.68	0.50	0.13	0.36
K (AMS)	0.59	0.60	0.63	**0.77**	0.61	0.22	0.47
Primary pollutants							
PAH	0.48	0.60	**0.90**	**0.81**	0.37	-0.11	0.14
BC	0.63	0.56	**0.82**	**0.83**	0.69	0.18	0.50
CO	0.52	0.54	0.62	**0.74**	0.61	0.29	0.51
NO_2	0.45	0.64	0.61	**0.72**	0.57	0.20	0.44
AMS tracer ions (*m/z* value)							
CO_2^+ (44)	0.32	0.38	0.41	0.47	**0.84**	**0.75**	**0.92**
$C_2H_5N^+$ (43)	0.46	0.52	0.48	0.62	0.52	0.35	0.50
$C_2H_4O_2^+$ (60)	**0.70**	0.66	**0.85**	**0.92**	0.67	0.10	0.44
$C_3H_5O_2^+$ (73)	**0.71**	**0.76**	**0.74**	**0.94**	0.66	0.15	0.46
$C_3H_3O^+$ (55)	0.55	**0.86**	0.64	**0.88**	0.66	0.24	0.51
$C_3H_7^+$ (43)	**0.91**	**0.69**	0.63	**0.96**	0.46	0.02	0.27
$C_3H_7N^+$ (57)	0.60	0.57	0.56	**0.74**	**0.78**	0.33	0.63
$C_4H_7^+$ (55)	**0.85**	**0.78**	0.65	**0.98**	0.49	0.04	0.30
$C_4H_9^+$ (43)	**0.95**	0.62	0.61	**0.94**	0.42	0.00	0.24
$C_5H_{11}^+$ (57)	**0.96**	0.59	0.60	**0.92**	0.41	-0.01	0.23
$C_5H_8O^+$ (84)	0.58	**0.93**	0.54	**0.90**	0.50	0.09	0.33
$C_6H_{10}O^+$ (98)	0.57	**0.95**	0.51	**0.89**	0.41	0.02	0.24
$C_7H_{12}O^+$ (112)	0.57	**0.89**	0.58	**0.88**	0.53	0.09	0.35
$C_9H_7^+$ (115)	**0.82**	**0.74**	**0.72**	**0.96**	0.18	-0.05	0.10
CHN^+ (27)	0.47	0.47	0.58	0.63	**0.73**	0.53	**0.73**
CN^+ (26)	0.35	0.35	0.46	0.48	0.57	0.42	0.57
$CH_2SO_2^+$ (77)	0.30	0.24	0.37	0.37	**0.83**	0.53	**0.79**
$CH_3SO_2^+$ (78)	0.37	0.27	0.41	0.44	**0.91**	0.54	**0.83**

BC, black carbon; AMS, aerosol mass spectrometer; PAH, polycyclic aromatic hydrocarbons
Value that are r > 0.7 are boldfaced

Table 3. Comparison of aerosol properties and meteorological parameters between the high loading and low loading periods.

	High PM loading	Low PM loading
Average non-refractory submicrometer particulate matter ($NR\text{-}PM_1$) mass concentration ($\mu g\ m^{-3}$) (Average ± 1σ)	43.6 ± 2.4	12.6 ± 7.1
O/C (H/C) ratio*	0.36 (1.82)	0.41 (1.75)
Trace gas conc.(CO (ppm) and /NO_2/O_3/SO_2 (ppb))	1.2/56/61/7.5	0.5/30/18.4/6.4
Temperature (°C) (average ± 1σ)	2.5 ± 3.4	-2.8 ± 4.4
RH (%) (average ± 1σ)	71 ± 15	50 ± 12

*calculated using the improved Canagaratna-ambient method (Canagaratna et al., 2015).

PM, particulate matter; $NR\text{-}PM_1$, non-refractory submicrometer particulate matter; RH, relative humidity

Figures

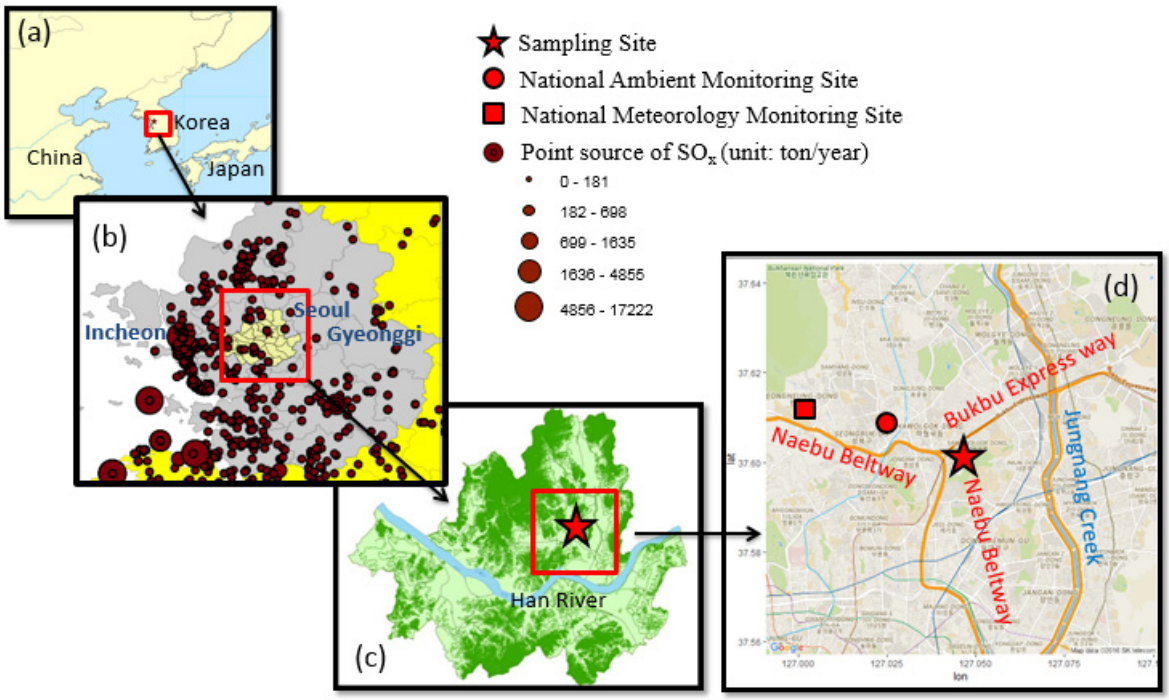

Figure 1. (a) The map of Korea, showing the location between China and Japan; **(b)** Seoul (light yellow) surrounded by other nearby cities including Incheon and Gyeonggi Province (Grey area) where industrial facilities are located (west) and agricultural areas are sporadically located surrounding Seoul. Location of point source of SO_x are indicated by dark red circles (Size: Concentration). Agricultural areas are sporadically located at East; **(c)** The location of sampling site in Seoul which is at the north-east of the center of Seoul and north of Han river; **(d)** The indications of sampling site. Next to sampling site, Bukbu express highway is located and residential and commercial areas are surrounding the sampling site.

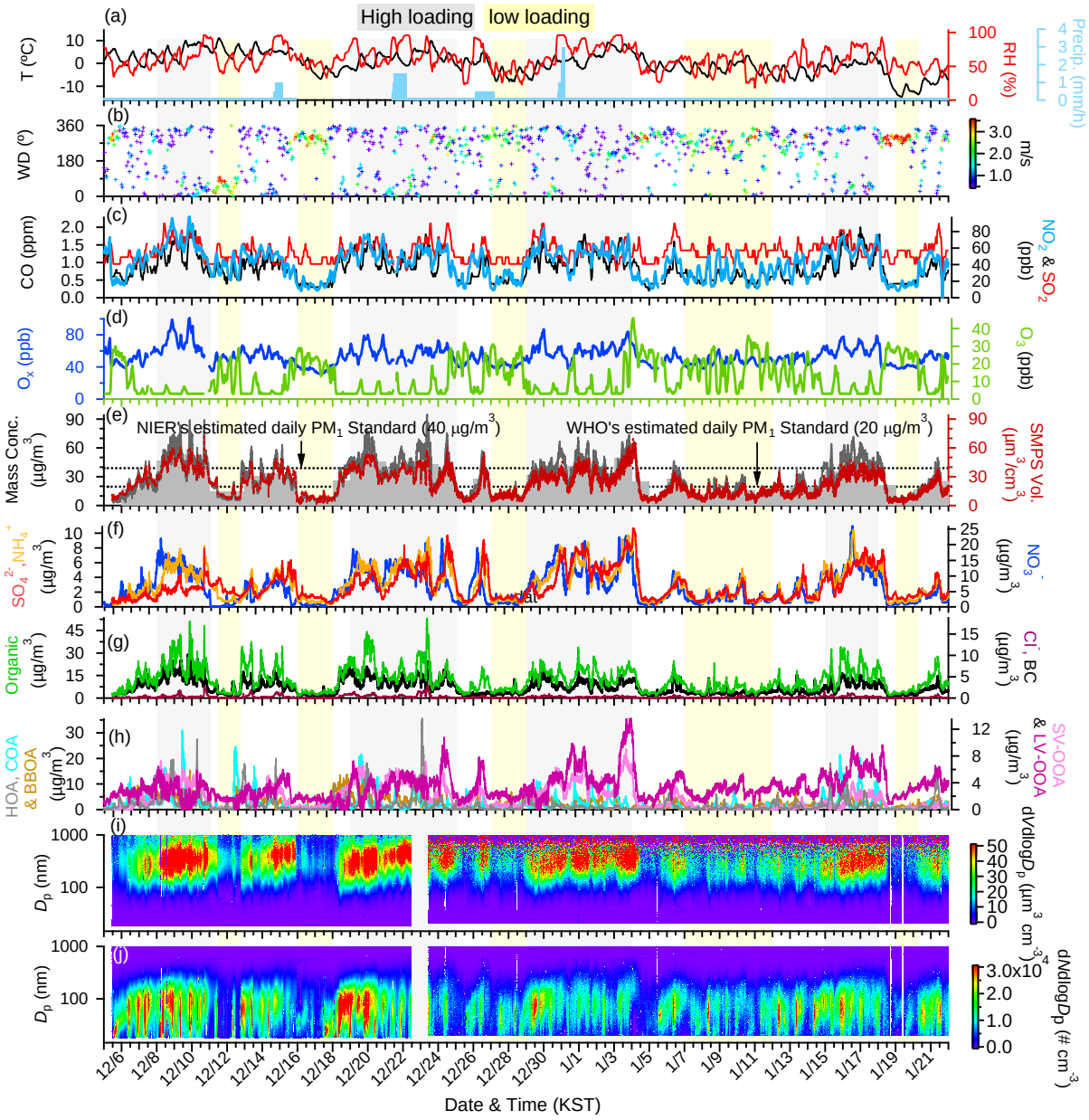
(a)
High loading
low loading
T (ºC)
RH (%)
Precip. (mm/h)
(b)
WD (º)
m/s
(c)
CO (ppm)
NO2 & SO2 (ppb)
(d)
Ox (ppb)
O3 (ppb)
(e)
NIER's estimated daily PM1 Standard (40 μg/m3)
WHO's estimated daily PM1 Standard (20 μg/m3)
Mass Conc. (μg/m3)
SMPS Vol. (μm3/cm3)
(f)
SO4 2-,NH4 +
NO3 -
(g)
Organic (μg/m3)
Cl-, BC (μg/m3)
(h)
HOA, COA & BBOA (μg/m3)
SV-OOA & LV-OOA (μg/m3)
(i)
Dp (nm)
dV/dlogDp (μm3 cm-3)
(j)
dN/dlogDp (# cm-3)
12/6
12/8
12/10
12/12
12/14
12/16
12/18
12/20
12/22
12/24
12/26
12/28
12/30
1/1
1/3
1/5
1/7
1/9
1/11
1/13
1/15
1/17
1/19
1/21
Date & Time (KST)

Figure 2. Overview of the temporal variations of submicron aerosols at the Korea Institute of Science and Technology (KIST) in Seoul from December 8, 2015 to January 21, 2016: **(a)** Time series of ambient air temperature (T), relative humidity (RH), solar radiation (SR), and precipitation (Precip.); **(b)** Time series of wind direction (WD), with colors showing different wind speeds (WS); **(c)** Time series of CO,SO_2, and NO_2; **(d)** Time series of O_x (NO_2 + O_3) and O_3; **(e)** Time series of total particulate matter (PM_1),scanning mobility particle sizer (SMPS) volume concentrations Also shown are the 24 h averaged PM_1+BC with bars. Estimated NIER's and WHO's daily PM_1 standards (40 μg/m^3 and 20 μg/m^3, respectively) are also shown with dashed line for the comparisons; **(f)** Time series of the organic aerosols (Org.), nitrate (NO_3^-), sulfate (SO_4^{2-}), ammonium (NH_4^+), chloride (Cl^-), and BC; **(g)** Time series of the total organic aerosol (OA) of the five factors derived from the positive matrix factorization (PMF) analysis (see section 3.3) **(h,i)** Particle volume and number size distributions by SMPS. Shaded regions indicate the persistent (> 2days) high loading (gray) and low loading (yellow) periods when daily average conc. > 30 μg/m^3 and <14 μg/m^3, respectively.

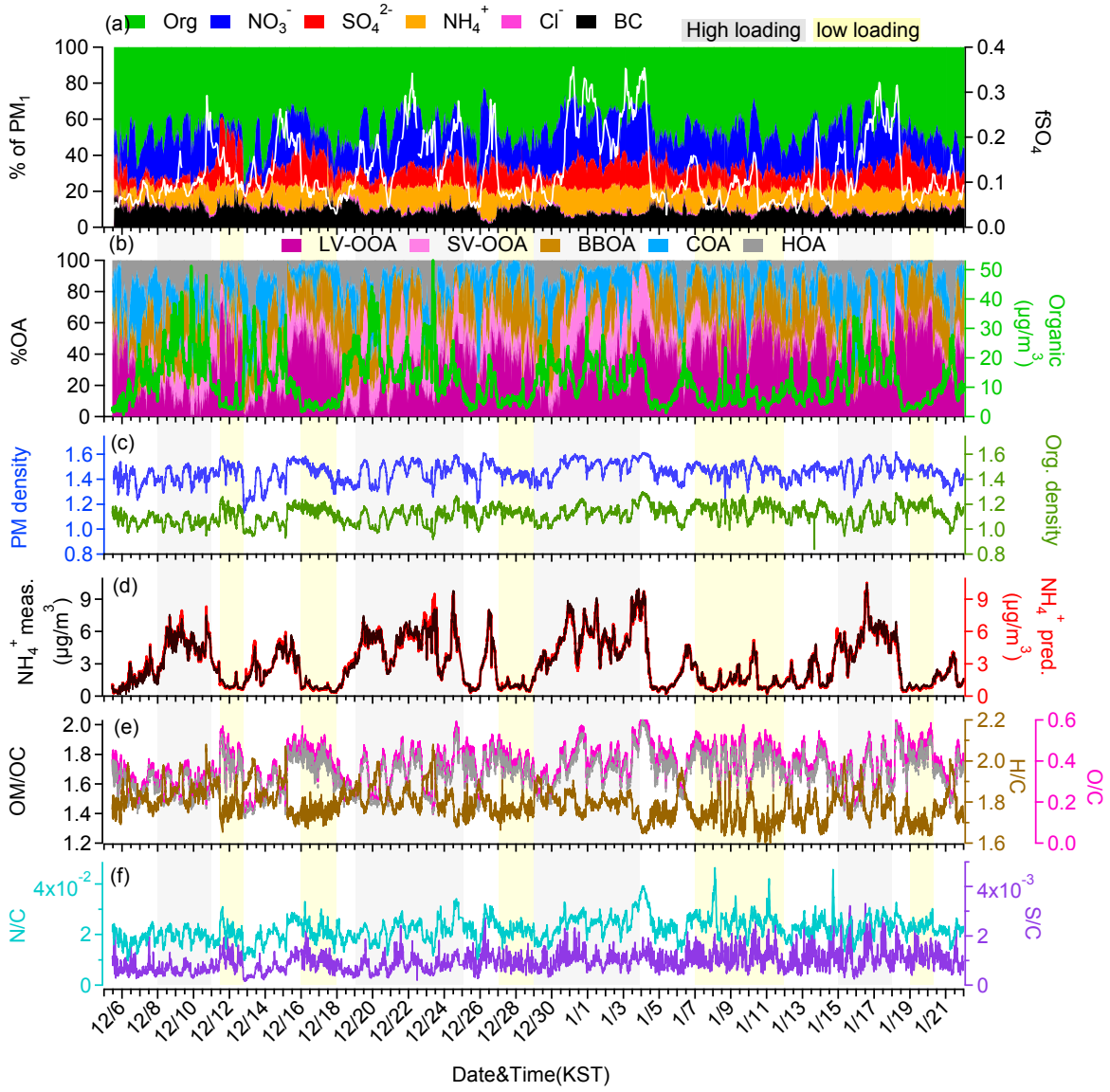

Figure 3. Overview of the chemical composition of submicron aerosols at the Korea Institute of Science and Technology (KIST) in Seoul from December 8, 2015 to January 21, 2016: **(a)** Time series of the mass fractional contribution of organic aerosols (Org.), nitrate (NO_3^-), sulfate (SO_4^{2-}), ammonium (NH_4^+), chloride (Cl^-), and BC to total PM_1 Also shown is the time series of f SO_4 (ratio of $SO_4^{2-}/(SO_2+ SO_4^{2-})$)with the fraction of SO_4^{2-} to the concentration of ; **(b)** Time series of the mass fractional contribution to total organic aerosol (OA) of the five factors derived from the positive matrix factorization (PMF) analysis (see section 3.3), and the time series of the organic aerosols; **(c)** Time series of the organic density estimate using the method reported in (Kuwata et al., 2012) with bulk aerosol density using the organic density estimated in this figure; **(d)** Time

series of the measured and predicted NH_4^+ concentrations; **(e, f)** organic matter to organic carbon (OM/OC), oxygen to carbon (O/C), hydrogen to carbon (H/C), nitrogen to carbon (N/C), and sulfur to carbon (S/C) ratios of OA, where the O/C, H/C and OM/OC elemental ratios were determined using the updated method (Canagaratna et al., 2015).

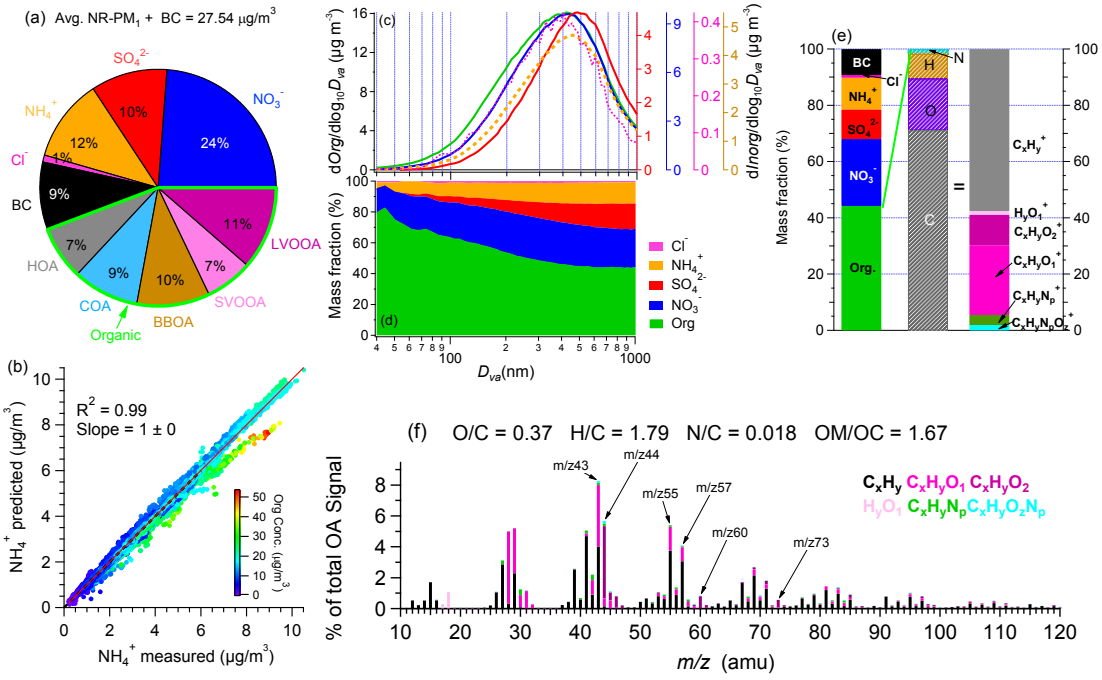

Figure 4. (a) Average compositional pie chart of PM_1 species (non-refractory-PM_1 plus black carbon (BC)) and each of the OA factors over the whole campaign. The green outline indicates the fraction of total OA; **(b)** Scatterplot that compares predicted NH_4^+ versus measured NH_4^+ concentrations. The predicted values were calculated assuming full neutralization of the anions (e.g., sulfate, nitrate, and chloride). The data points are colored by organic concentrations.; **(c)** Campaign-averaged size distributions for individual NR-PM_1 species; **(d)** Averaged mass fractional contributions of each NR-PM_1 species to the total NR-PM_1 mass as a function of size. ; **(e)** Overview of the average PM_1 and OA compositions in Seoul during winter; **(f)** Average high-resolution mass spectrum of OA colored by the different ion families. The average elemental ratios for the OA fraction are described.

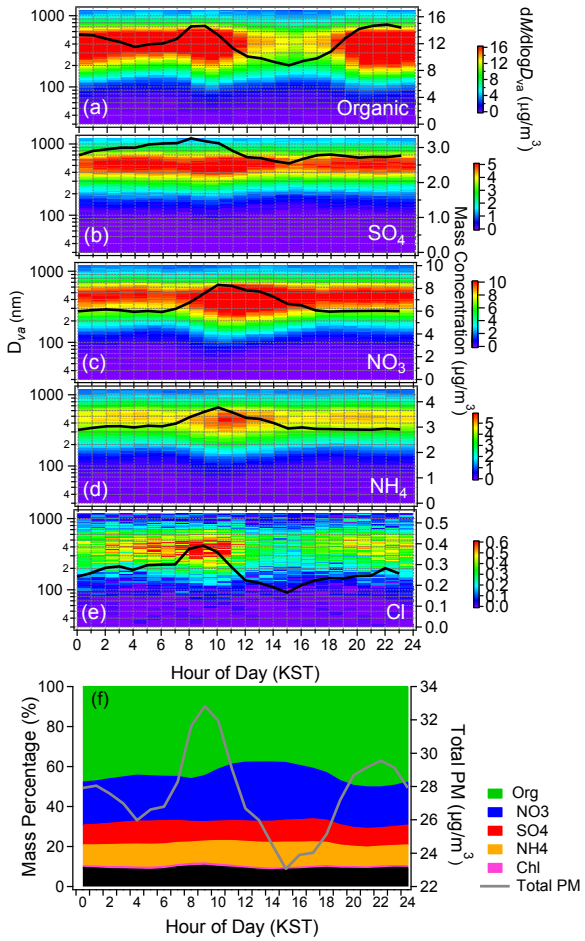

Figure 5. (a–e) One-hour averaged diurnal profiles of mass-based size distributions of each of the non-refractory submicrometer particulate matter (NR-PM_1) species colored by their mass concentration (left axis; D_{va}, vacuum aerodynamic diameter) and average diurnal profiles of each of the PM_1 species (right axis); **(f)** Average diurnal mass fractional contribution of each of PM_1 species to the total PM_1 diurnal mass and the total PM_1 mass loading

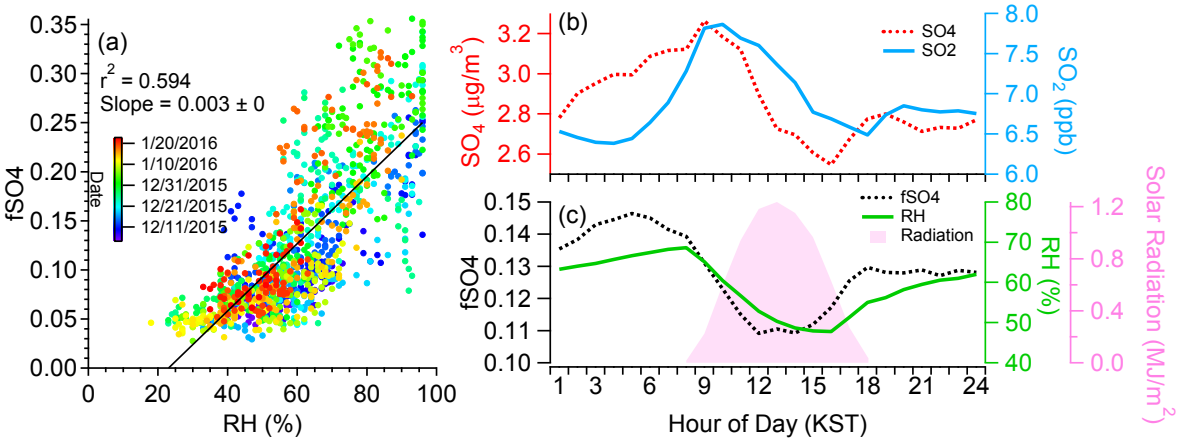

Figure 6. (a) Scatterplot of the variations of fSO_4 ratios as a function of RH **(b)** One-hour averaged diurnal profiles of SO_2 and SO_4 and **(c)** One-hour averaged diurnal profiles of fSO_4, RH and solar radiation. The solar radiation measurement site is located at 20km away from the measurement site.

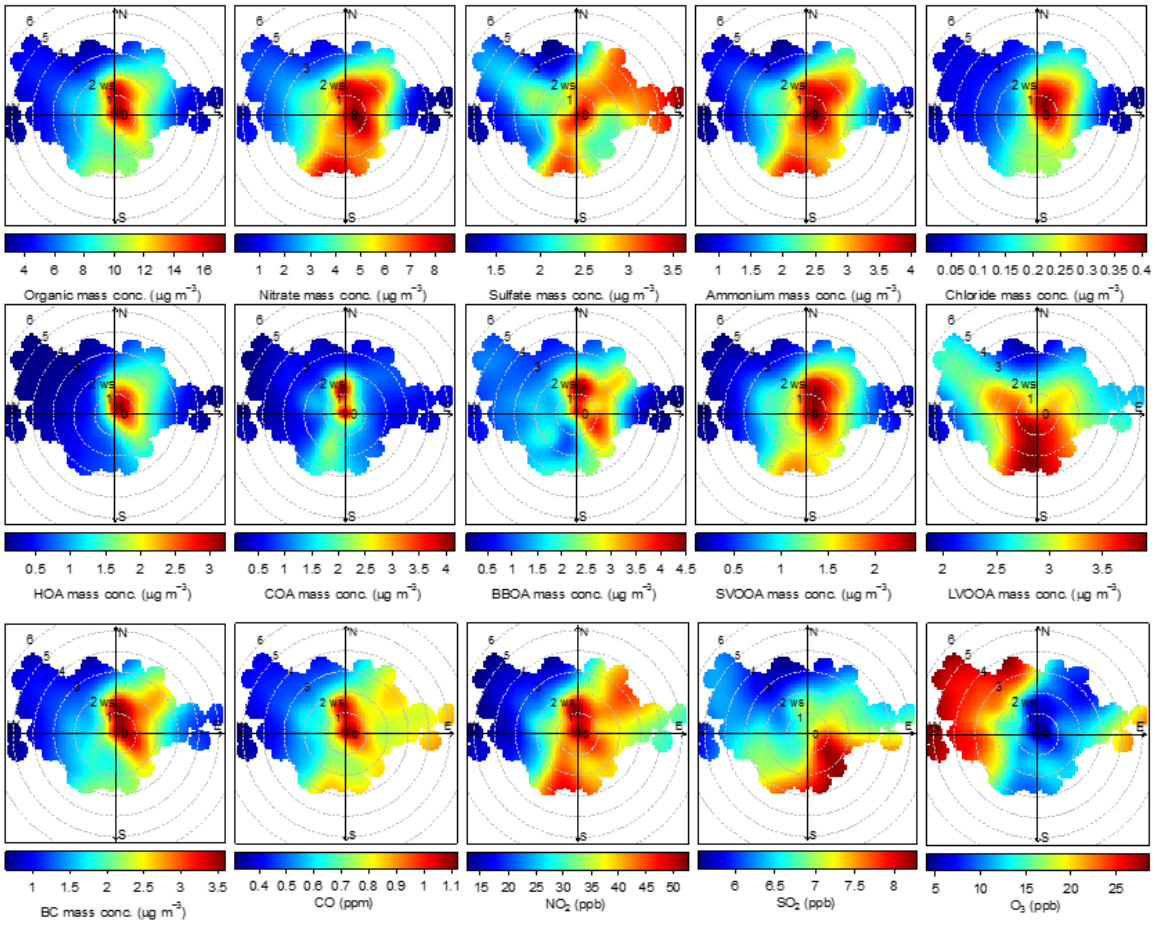

Figure 7. Polar plots of hourly averaged PM_1 species concentrations (top row), mass concentrations of the five OA factors identified from PMF analysis (middle row), and the mixing ratios of various gas phase species as a function of WS and direction.

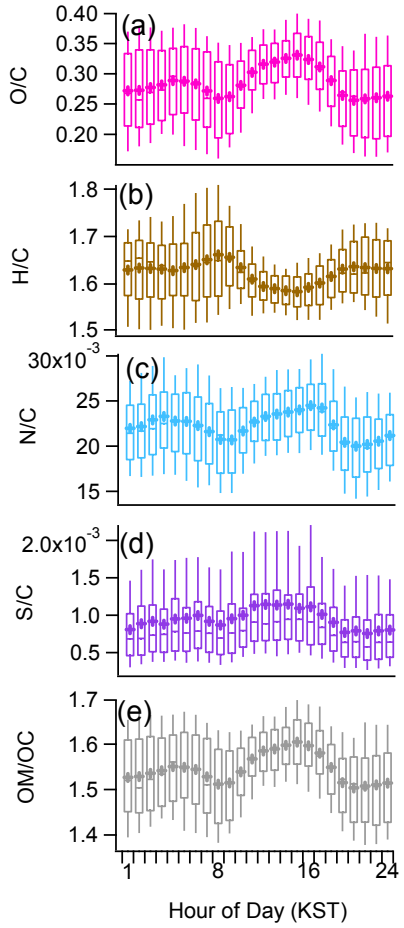

Figure 8. (a–e) Average diurnal profiles of the organic matter to organic carbon (OM/OC), oxygen to carbon (O/C), hydrogen to carbon (H/C), nitrogen to carbon (N/C), and sulfur to carbon (S/C) ratios of OA, where the O/C, H/C and OM/OC elemental ratios were determined using the updated method (Canagaratna et al., 2015).

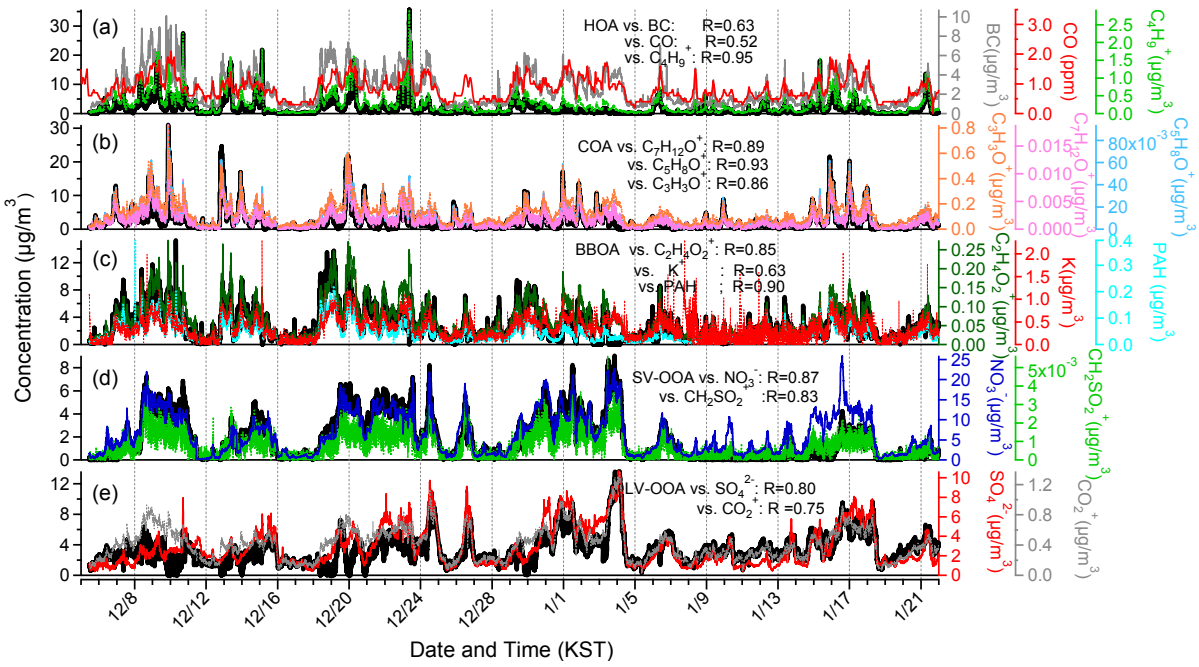

Figure 9. Overview of the results from PMF analysis including the time series of each of the OA factors and various tracer species.

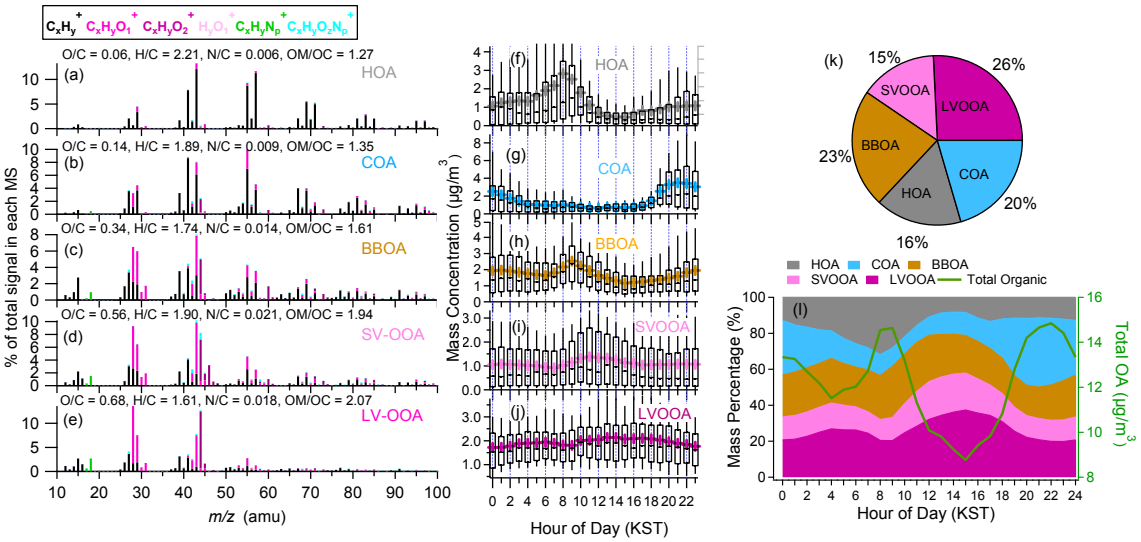

Figure 10. Overview of the results from PMF analysis including high-resolution mass spectra of the **(a)** Hydrocarbon-like organic aerosol (HOA), **(b)** Cooking OA (COA), **(c)** Biomass burning OA (BBOA), **(d)** Semi volatile oxygenated OA (SV-OOA), and **(e)** Low volatility oxygenated OA (LV-OOA) colored by different ion families; **(f–i)** Average diurnal profiles of each of the OA factors (the 90th and 10th percentiles are denoted by the whiskers above and below the boxes, the 75th and 25th percentiles are denoted by the top and bottom of the boxes, the median values are denoted by the horizontal line within the box, and the mean values are denoted by the colored markers); **(k)** Compositional pie chart of the average fractional contribution of each of the OA factors to the total OA over the campaign; **(l)** Average diurnal mass fractional contribution of each of the OA factors to the total OA diurnal mass and the total OA mass loading.

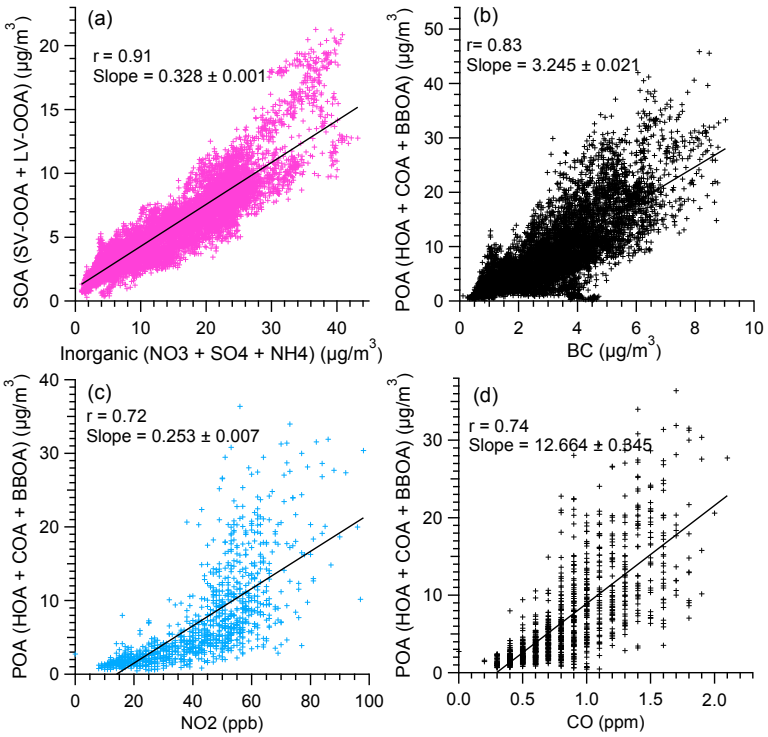

Figure 11. Scatterplot between: **(a)** SOA and sum of inorganic (NO_3 + SO_4 + NH_4) **(b)** POA and BC; **(c)** POA and NO_2; and **(d)** POA and CO

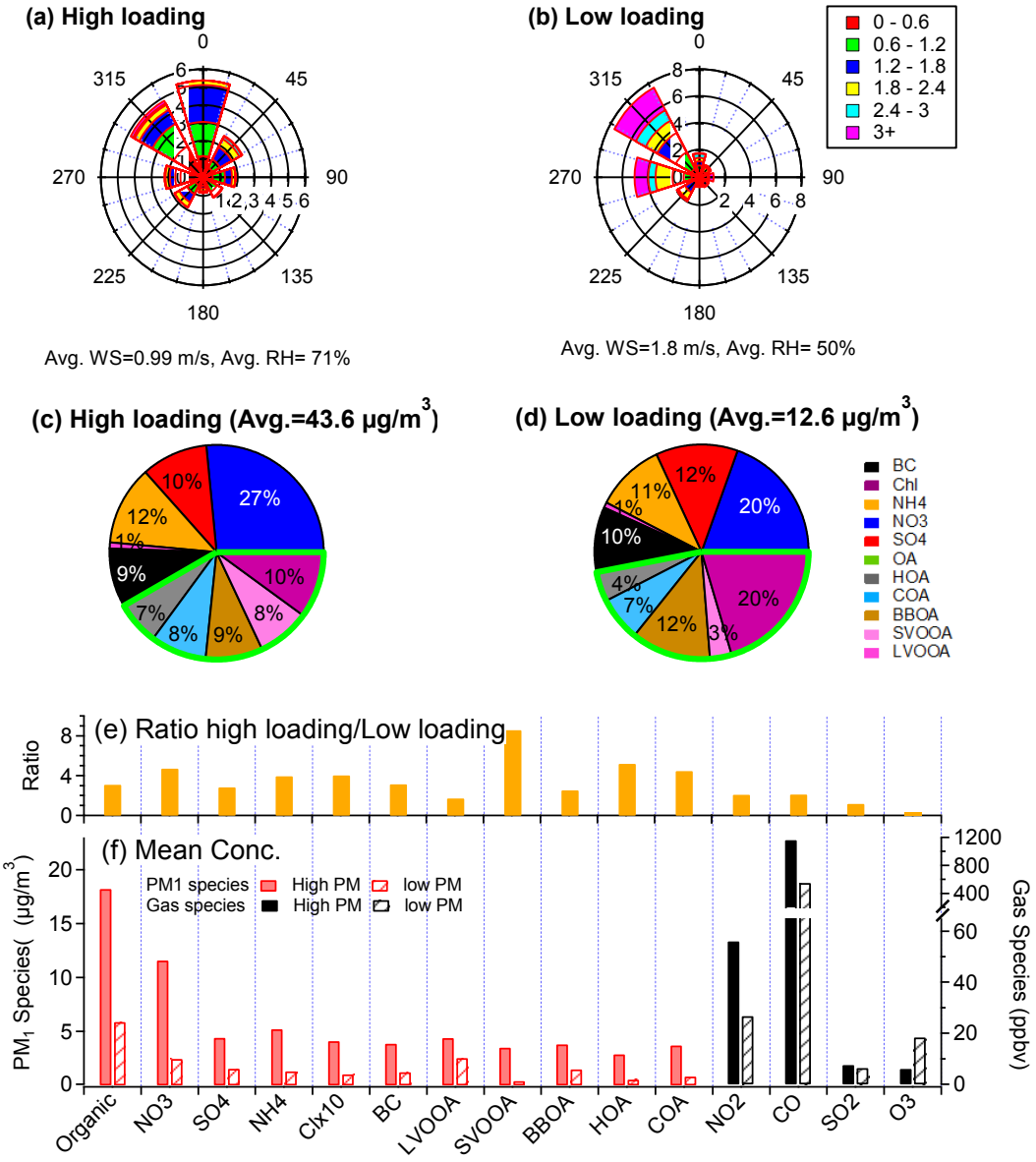

Figure 12. Comparisons of averaged properties measured during high particulate matter (PM), loading and low PM loading periods; **(a,b)** Wind rose plots, colored by wind speed for each different period; **(c,d)** fractional contributions of each species to the total PM_1 (non-refractory-PM_1 plus BC) mass; **(e)** ratios of absolute concentrations of each PM_1 and gas species during high loading and low loading periods; **(f)** Comparisons of averaged absolute concentrations of PM_1 species and gaseous pollutants for each different period.

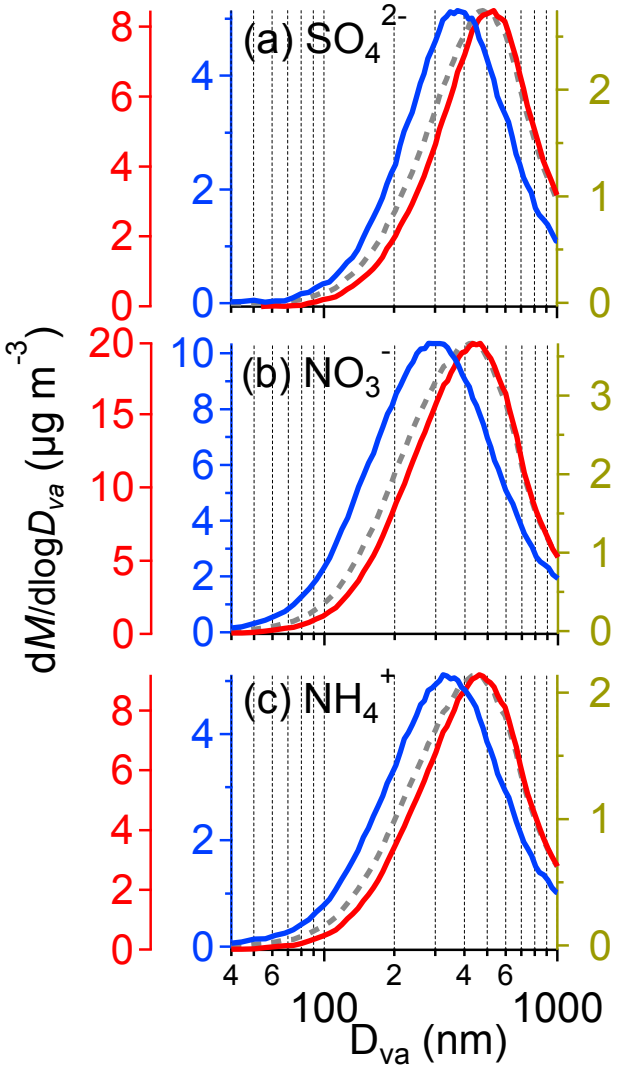

Figure 13. Averaged mass-based size distributions of **(a)** sulfate, **(b)** nitrate, and **(c)** ammonium during the entire (broken grey curve), high PM (red curve), and low PM (blue curve) periods as marked in Fig. 2 and 3.

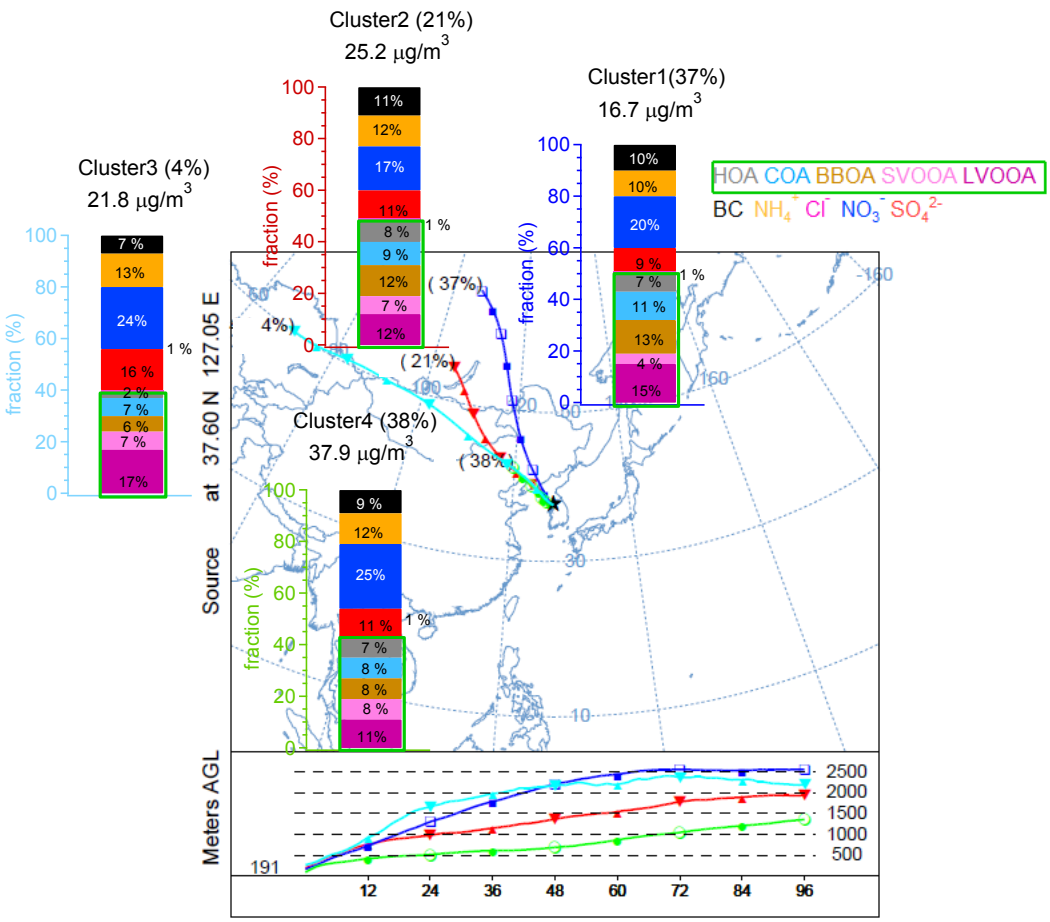

Figure 14. Averaged compositional bar graph of PM_1 species (non-refractory-PM_1 plus black carbon (BC)) and each of the OA factors in different clusters from the four cluster solution. The trajectories were released at half of the mixing height at the KIST (latitude: 37.60N; longitude: 127.05E) and the average arriving height for the back trajectories for this study was approximately 191 m.